Rochester Institute of Technology

RIT Digital Institutional Repository

Theses

11-2-2009

Anisotropic acid catalyst displacement in a chemically amplified photoresist via application of an electric field

Ward A. Johnson

Follow this and additional works at: https://repository.rit.edu/theses

Recommended Citation

Johnson, Ward A., "Anisotropic acid catalyst displacement in a chemically amplified photoresist via application of an electric field" (2009). Thesis. Rochester Institute of Technology. Accessed from

Anisotropic Acid Catalyst Displacement in a Chemically Amplified Photoresist via Application of an Electric Field

By

Ward A. Johnson

A Thesis Submitted

In Partial Fulfillment

Of the Requirements for the Degree of

Master of Science

in

Microelectronic Engineering

Approved by:

Prof. _____
      Dale E. Ewbank (Thesis Advisor)

Prof. _____
      Dr. Bruce W. Smith (Thesis Committee Member)

Prof. _____
      Dr. Thomas W. Smith (Thesis Committee Member)

DEPARTMENT OF MICROELECTRONIC ENGINEERING

COLLEGE OF ENGINEERING

ROCHESTER INSTITUTE OF TECHNOLOGY

ROCHESTER, NEW YORK

NOVEMBER 2, 2009

Acknowledgment

Abstract

Electrostatic force theory and Fickean diffusion theory both predict that anisotropic movement can be conveyed to chemically amplified resist (CAR) acid catalysts via an electric field during the post exposure bake (PEB). A demonstration of this effect was attempted through photoresist thickness loss measurements with and without the addition of an electric field. The experimental design underwent multiple evolutionary iterations and measured as much as 86 nm of additional thickness loss with the presence of an electric field compared to a PEB control. Repeatability was inconsistent and several principal assumptions were found to be in violation. From measurements of current across exposed photoresist during an electric field enhanced post exposure bake (EFE-PEB), it was concluded that acid pileup at the electrode/photoresist interfaces caused charge separation which reduced the internal electric field; this effect was relieved by acid neutralization via electrons from the cathode.

Table of Contents

List of Tables

List of Figures

List of Acronyms

AC .... alternating current

ARC .... anti reflection coating

BARC .... bottom anti reflection coating

CAR .... chemically amplified resist

DC .... direct current

DI .... deionized

DUV .... deep ultraviolet

EFE-PEB .... electric field enhanced post exposure bake

ESCAP .... environmentally stable chemically amplified photoresist

FTIR .... frustrated total internal reflection

ITRS .... international technology roadmap for semiconductors

LER .... line edge roughness

LWR .... line width roughness

MPU .... microprocessor unit

NA .... numerical aperture

PAG .... photoacid generator

PEB .... post exposure bake

PECVD .... plasma enhanced chemical vapor deposition

SIL .... solid immersion lithography

TARC .... top anti reflection coating

TEOS .... tetraethyl orthosilicate

TIR .... total internal reflection

TMAH .... tetramethylammonium hydroxide

Chapter 1

Rationale

Relating to chemically amplified photoresists, the conditions that define line width roughness and standing wave effects are attributable to the 3-dimensional spatial distribution of the acid catalyst. The number of interactions those acid ions have with other resist molecules is directly attributable to the quantum efficiency of the process. The surface imaging limitations of solid immersion lithography (SIL) are caused by resist absorption and a large optical path length due to the oblique interference angles involved; however, acid catalyst is generated and so, like the line width roughness, standing wave effects, and quantum efficiency, the latent image can be altered by moving the catalyst about those 3 dimensions.

Thermal processes relieve these effects by diffusing the acid isotropically (movement in 3 spatial dimensions). If a drift component could be appended to the acid's velocity, unexposed areas of the photoresist could be deprotected selectively and with greater precision than a Gaussian distribution, which is characteristic of a thermal process, allows. Oscillating the acid catalyst within a narrowly defined region would also increase quantum efficiency by multiplying the number of deprotected inhibitors; by this same token, a single catalyst molecule could deprotect a region spanning the entire thickness of the photoresist.

Influencing acid catalyst diffusion concurrently with the exposure, as opposed to during a post exposure bake (PEB), would eliminate a lengthy process step and further increase wafer throughput. This process would require a low activation photoresist, while

field application during the PEB would be compatible with either low or high activation energies.

1.1 Line Width Roughness

The 2007 edition of the International Technology Roadmap for Semiconductors (ITRS) states that there are no known manufacturable solutions capable of printing features with low frequency line width roughness (LWR), within 3 standard deviations, at or below 2.7 nm; this is the predicted requirement for microprocessor units (MPU) in 2009. The portion of the ITRS apropos LWR is shown in Fig. 1.1.

Year of Production	2007	2008	2009	2010	2011	2012	2013	2014	2015
DRAM ½ pitch (nm) (contacted)	65	57	50	45	40	36	32	28	25
Flash ½ pitch (nm) (un-contacted poly)	53.5	45.0	40.1	35.7	31.8	28.3	25.3	22.5	20.0
MPU/ASIC Metal 1 (M1) ½ Pitch (nm)(contacted)	68	59	52	45	40	36	32	28	25
MPU physical gate length (nm) [after etch]	25	23	20	18	16	14	13	11	10
MPU gate in resist length (nm)	42	38	34	30	27	24	21	19	17
Resist Characteristics *									
Resist meets requirements for gate resolution and gate CD control (nm, 3 sigma) **†	2.6	2.3	2.1	1.9	1.7	1.5	1.3	1.2	1.0
Resist thickness (nm, single layer) ***	105-190	90-160	80-145	70-130	60-115	55-100	50-90	45-80	40-75
PEB temperature sensitivity (nm/C)	1.75	1.5	1.5	1.5	1.5	1.5	1	1	1
Backside particle density (particles/cm^2)	0.28	0.28	0.28	0.28	0.28	0.28	0.28	0.28	0.28
Back surface particle diameter: lithography and measurement tools (nm)	120	120	100	100	100	100	75	75	75
Defects in spin-coated resist films (#/cm^2) †	0.01	0.01	0.01	0.01	0.01	0.01	0.01	0.01	0.01
Minimum defect size in spin-coated resist films (nm)	40	35	30	30	20	20	20	20	10
Defects in patterned resist films, gates, contacts, etc. (#/cm^2)	0.04	0.03	0.03	0.03	0.02	0.02	0.02	0.02	0.01
Minimum defect size in patterned resist (nm)	40	35	30	30	20	20	20	20	10
Low frequency line width roughness: (nm, 3 sigma) <8% of CD *****	3.4	3.0	2.7	2.4	2.1	1.9	1.7	1.5	1.3
Defects in spin-coated resist films for double patterning (#/cm^2)	0.005	0.005	0.005	0.005	0.005	0.005	0.005	0.005	0.005
Backside particle density for double patterning (#/cm^2)	0.14	0.14	0.14	0.14	0.14	0.14	0.14	0.14	0.14

Manufacturable solutions exist, and are being optimized
Manufacturable solutions are known
Interim solutions are known
Manufacturable solutions are NOT known

Fig. 1.1. 2007 edition of the ITRS roadmap stating the maximum LWR to be 8% of the resist gate length. In 2009, MPUs will require 34 nm resist lines with LWR of no more than 2.7 nm; as shown in the key, no manufacturable solutions exist that can meet the LWR requirement [1].

Ordered motion of the acid catalyst would eliminate the localized lateral diffusion responsible for LWR, and an increased quantum efficiency would reduce the time allowable for diffusion to occur.

1.1.1 Reduction of Line Width Roughness

The anisotropy offered by the inclusion of an electric field not only improves the quantum efficiency of the exposed regions by multiplying the number of catalyst/resist interactions, but also inhibits deprotection in the unexposed regions by stunting the opportunity of the acid to diffuse laterally. An ancillary consequence of this increase in acid contrast is a reduction of line width roughness, which is defined in the literature section of this proposal.

The lateral motion of the acid catalyst follows Brownian motion. With no drift velocity, the catalyst's sphere of influence grows with respect to time; by limiting the radius of this sphere of influence by reducing lateral diffusion, distinguished areas of exposure are maintained, minimizing the roughness of the line.

1.2 Standing Wave Effects

Reflections off film stack interfaces cause interference effects that manifest both physically, as the cross section of the line, and in the form of sinusoidal process variations. Post exposure bakes and bottom and top anti reflection coatings (BARC and TARC), which involve additional process steps and the purchase of additional materials, are currently employed to reduce these effects.

1.2.1 Image Cross Section

At high angles indicative of hyper numerical aperture (NA) imaging, constructive

and destructive interference induces a sequence of well-defined anti-nodes. These areas

of constructive interference are nearly circular in their cross section and repeat from the

substrate/resist interface surrounded by a background of destructive interference; the

sharp intensity delineation produces antinodes within the intended features (spaces in the

case of a positive resist and lines in the case of a negative resist), causing bridging

structures to form between lines.

Isotropic thermal diffusion of the acid catalyst, existing in isolated areas

(separated by tens of nm) before the PEB, causes pockets of soluble resist to develop, and

in this way the spaces encroach upon the lines at evenly spaced intervals along the height

of the features, which leads to pattern collapse; these consequences are apparent in

Fig. 1.2.
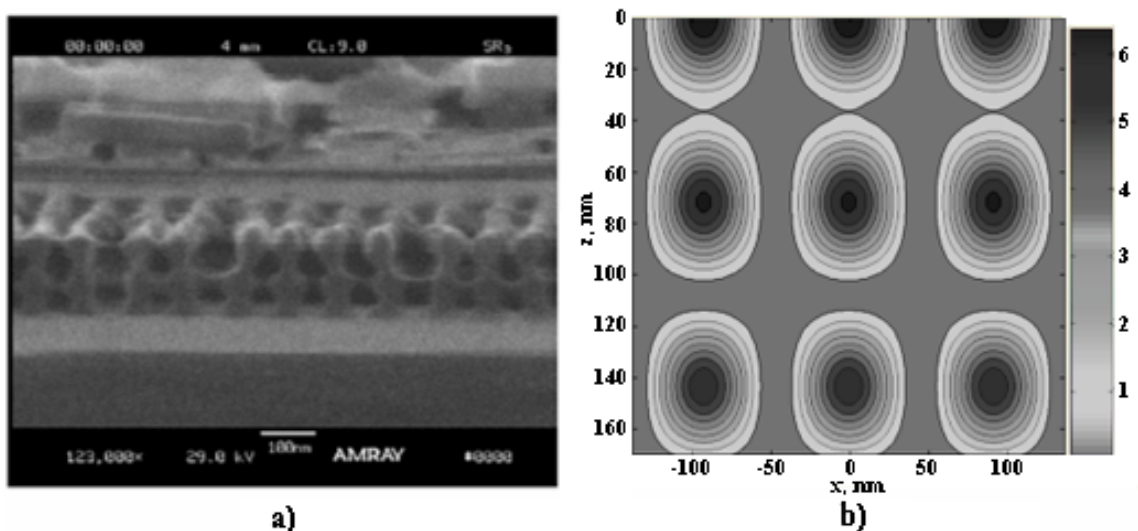
Fig. 1.2. a) Lines imaged at 1.05NA without the use of BARC. Standing waves result in sidewalls so severely lobed, the topcoat layer must be left intact to prevent pattern collapse. b) Simulation of imaging conditions shown in cross section; grayscale indicates radiation intensity. Both a) and b) are modified for clarity from [2].

Zhou, Fan, and Smith imaged lines at 1.05NA without the use of a BARC layer. Table I describes the film stack. The sidewall angles and simulated intensity map shown in Fig. 1.2 directly illustrate standing wave effects [2].

TABLE 1.1
FILM STACK USED IN NANOSPHERE FABRICATION [2]

Layer	Material	Complex refractive index	Thickness
Topcoat	TSP3A	1.414	40 nm
Resist	TOK012	1.71-0.039i	170 nm
Substrate	Silicon Wafer	0.87-2.76i	-

1.2.2   Process Robustness and Swing Effects

As exposure varies with depth into the resist, so does the development rate and imaged feature size. In addition, due to the sinusoidal nature of electromagnetic radiation, resist thickness fluctuation will result in different rates of change in dose requirements; in this manner, stable resist thicknesses that occur at the minimum and maximum values of the local process variation, with respect to change in dose requirements, repeat every half wavelength of the exposing radiation in the medium. Stability coincides with these values because the dependant variable rate of change is zero. As demonstrated in Fig. 1.3, this is still the case even with the use of standing wave reduction techniques.
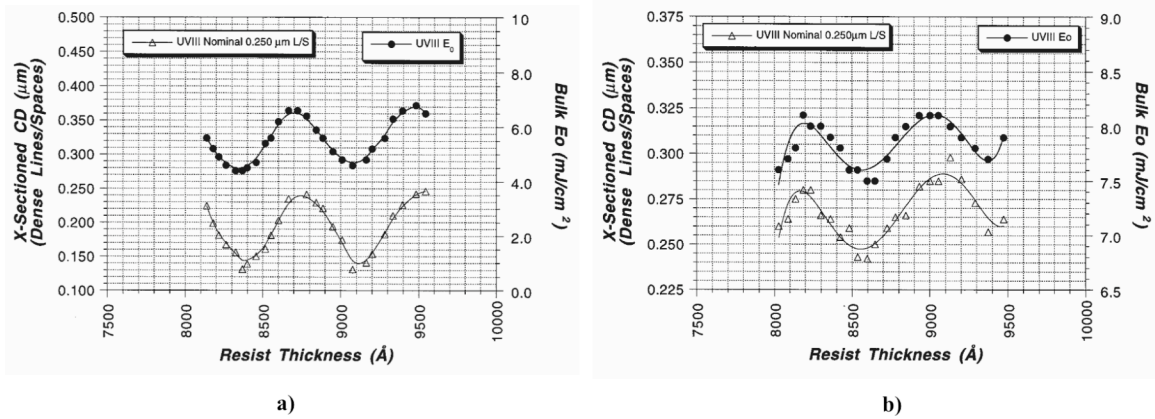
Fig. 1.3. Critical dimension and dose-to-clear swing curves of UVIII, a chemically amplified deep ultraviolet (DUV) photoresist, spin coated on a) a bare silicon wafer and b) a BARC layer on silicon. Modified for clarity from [3].

1.2.3 Imaging Sans Anti-Reflective Coatings

At large numerical apertures, the angular difference between pitches necessitates a multilayer BARC because one layer cannot be optimized for a range of angles of illumination; this action is shown in Fig. 1.4 [15].
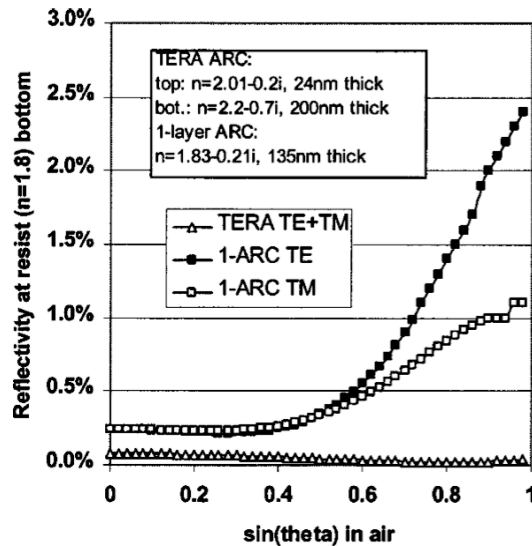
Fig. 1.4. A plot of reflectivity vs. reflection angle for single layer BARC and tunable etch-resistant (TERA) anti reflection coating (ARC), which is a two-layer BARC [15].

As illustrated in Fig. 1.2, the areas of positive interference of the exposing radiation are stacked vertically atop each other. These areas of intensity render the highest acid concentration with the surrounding nodes generating negligent amounts of catalyst. The collimated spheres of localized acid ostensibly lend themselves to an asymmetrical diffusion. Successfully developed features imaged at a hyper-NA without an ARC would support the asymmetrical diffusion hypothesis.

1.2.4   Increased Process Robustness

Additionally, standing waves become apparent in the form of process variation. These swings, shown in Fig. 1.3, can be used to quantify the effectiveness of any standing wave countermeasures, and a superposition of these plots, generated under different treatment conditions, would make any improvements pronounced.

1.3   Wafer Throughput

Because the lithography step is required more frequently than any other operation in the microfabrication of semiconductor devices, the speed at which exposure takes place directly correlates to a product's throughput. Given a constant source intensity, the dose-to-size is controlled by the exposure time, which is in turn determined by the sensitivity of the resist (and more specifically, in the case of chemically amplified resists, the quantum efficiency). A long exposure time correlates to a larger bottleneck at the lithography phase of microfabrication. However, a large quantum efficiency can be undesirable since a small dose results in a larger shot noise (fewer photons reduce the averaging effect on the spatial distribution), which would in turn increase the LWR.

1.3.1 Increased Quantum Efficiency

Increasing the acid catalyst diffusion length, albeit in one spatial dimension only, has the effect of increasing the number of possible deprotection reactions with the resist, and therefore increases the sensitivity of the reaction. The quantum efficiency, defined as the number of deprotected resist molecules per absorbed photon, is a metric of the photoresist sensitivity.

Increasing the sensitivity of a lithographic procedure has the effect of reducing the number of photons needed to expose to the resist in order to achieve equivalent results. Because photon exposure is a function of time, a more sensitive lithography process will reduce exposure time, increasing throughput.

1.4 Solid Immersion Lithography Beyond FTIR Limits

If the index of refraction of the final optical medium in an exposure system is larger than the index of refraction of the medium separating it from the photoresist, it is possible for total internal reflection (TIR) to occur inside the lens. The onset of TIR manifests at the critical angle θ_c, defined in equation 1 where, between the two media, n_l is the low refractive index and n_h is the high refractive index [4].

$$\theta_c = \sin^{-1}\left(\frac{n_l}{n_h}\right) \qquad (1)$$

Beyond the critical angle, an inhomogeneous surface wave emerges along the boundary of the lens and resist; this evanescent field couples electrons in the lens

8

responding to the internally reflected radiation with electrons in the photoresist. In this manner, the photoresist allows energy to traverse the separating medium; this mechanism is known as frustrated total internal reflection (FTIR). Equation 2 describes the amplitude of the evanescent wave over a distance z were λ is the radiation wavelength, α is the absorption of the medium, and θ is the angle of illumination in n_h [4].

$$A(z) = \exp\left[-z\left(\frac{2\pi n_h}{\lambda}\left(\sin^2\theta - \left(\frac{n_l}{n_h}\right)^2\right)^{\frac{1}{2}} + \alpha\right)\right] \tag{2}$$

When the numerical aperture exceeds the value of the index of refraction of the resist, the evanescent field is no longer frustrated by the photoresist, and so is no longer perturbed into propagation on the other side of the separating medium. Instead, the evanescent field continues to decay exponentially, which limits imaging to a depth of only a fraction of the wavelength, as shown in Fig. 1.5, and prevents the develop step from clearing resist material all the way down to the substrate.
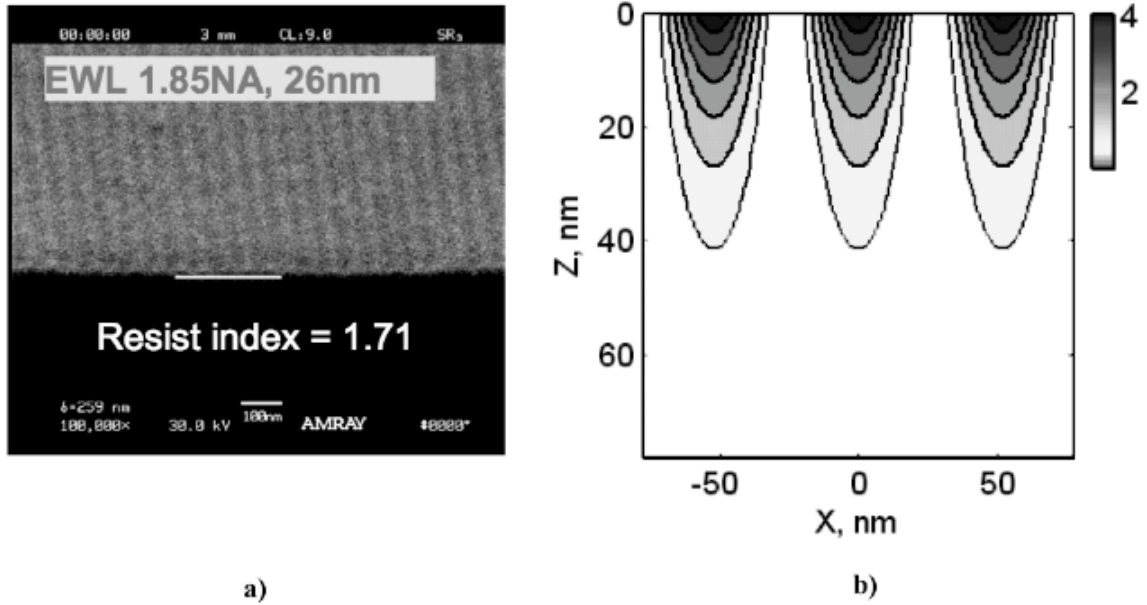
Fig. 1.5. a) 26 nm lines imaged at 1.85NA using solid immersion lithography and a sapphire prism b) Simulation of imaging conditions shown in cross section; grayscale indicates radiation intensity. Modified for clarity from [4].

1.5 Historical Experiments

Mosong Cheng and Andrew Neureuther [5]–[8] of the Electronics Research Laboratory at the University of California, Berkeley, have applied 1-dimensional Fickean diffusion and drift current equations to the partial differential equations describing the post exposure bake model, demonstrated a reduced lateral acid diffusion through reduced bake time for both electron beam and DUV chemically amplified photoresists, and patented an electric field enhanced PEB (EFE-PEB) method and apparatus. Sidewall angle results were varied. These papers were published between the years 2000 and 2004. In their three publications in the Journal of Vacuum Science and Technology [5]–[7], Cheng and Neureuther report superimposing an AC field over a DC field. The AC field was tested between 3.3 V and 10 V at frequencies from 0.07 Hz to 100 kHz. The DC field was tested between 0.85 V and 6.5 V.

337nm Space

$y = 114.87x - 342.12$

$y = 256.08x - 1305.6$
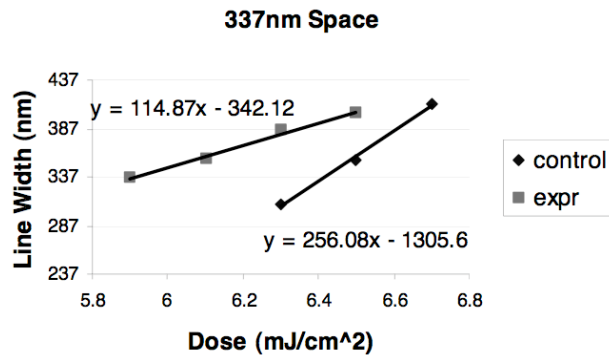
Fig. 1.6. Line width vs. dose for 337 nm on-mask spaces. The control group received no electric field during the PEB [9].
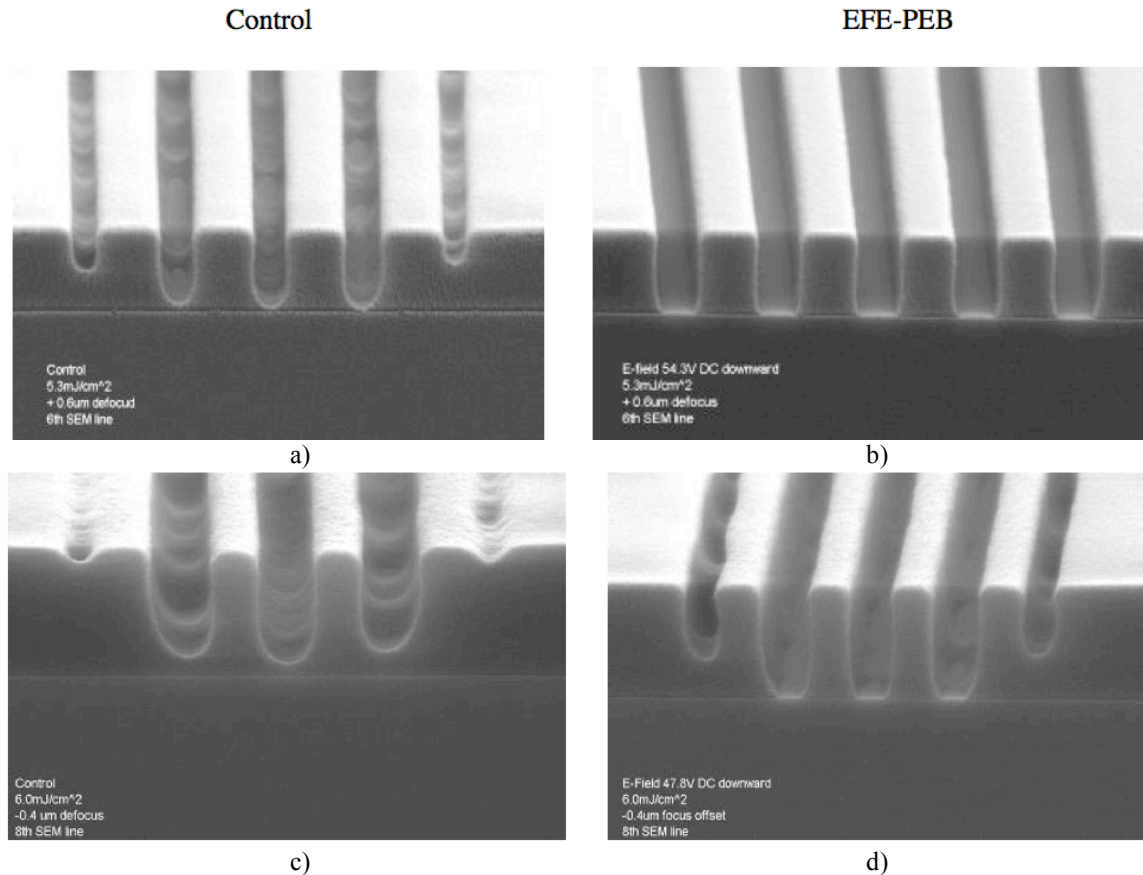
Fig. 1.7. An array of 5 1:1 lines exposed with identical doses. a) and b) show 500 nm lines with a +0.6 μm defocus. c) and d) show 337 nm lines exposed with a -0.4 μm defocus. The presence of an electric field during the PEB improves defocus tolerance in both cases [9].

11

In 2004, Jacob Poppe and Andrew Neureuther [9] of the Electronics Research Laboratory at the University of California, Berkeley, placed the electric potential generated by six 9 V batteries across the thickness of the photoresist and demonstrated an increase in focus latitude by 100 percent and a decrease in dose to clear by 8 percent. Poppe and Neureuther exposed 337 nm to 500 nm 5 line arrays with a 1:1 duty ratio into Apex-E photoresist with a 0.5 NA ASML KrF stepper. Dose-to-size data is presented in Fig. 1.6, and the cross sectional scanning electron microscopy (SEM) results depicting defocus process robustness are shown in Fig. 1.7.

As shown in Fig. 1.6, the addition of an electric field to the post exposure bake reduces the dose to size; this gives supporting evidence to the theory that an EFE-PEB increases the resist sensitivity by multiplying the quantum efficiency.

Chapter 2

Theory

2.1 DUV CAR Chemistry

Influencing the dimension and form of the soluble portion of chemically amplified photoresist with an electric field is possible after exposure has taken place because the solubility of the resist is changed via an acid-catalyzed deprotection reaction. Fig. 2.1 illustrates such a reaction.
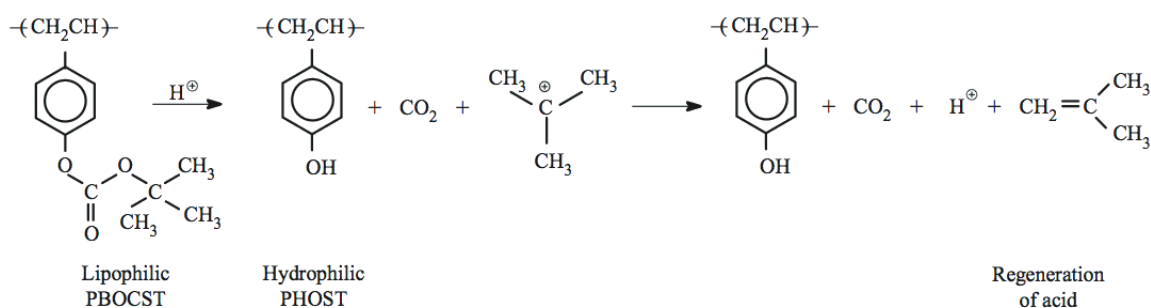
Fig. 2.1. Photoresist deprotection via acid catalyst. Upon cleavage of the pendant group, the lipophilic polymer becomes hydrophilic. Modified from [12].

The importance of the acid catalyzation is two-fold: an acid is a charged particle so its movement through space is in part governed by electrostatic behavior, and the fact that the acid serves as a catalyst means that additional exposure is unnecessary even though the hydrogen ions are being distributed over a larger area. Therefore few photoacid reactions can deprotect many resist molecules. These two factors allow an electric field to force a catalyst to move from point A to point B and deprotect resist molecules it interacts with along this path until the reaction is terminated by either a

quencher removing the catalyst from the reaction or the deprotection of all resist molecules within the diffusion length.

2.2 Drift and Diffusion

Equations 3 through 7 describe the kinetic behavior of a free hydrogen ion placed in an electric field generated by a parallel plate capacitor:

$$\left| \vec{E}_{//\,plate\,cap.} \right| = \frac{q_{per\,plate}}{\varepsilon_0 \cdot A} = \frac{V}{d} \tag{3}$$

$$\vec{F} = \vec{E} \cdot q_{acid} \tag{4}$$

$$\vec{F} = m_{acid} \cdot \vec{a} \tag{5}$$

$$\left| \vec{a}_{acid} \right| = \frac{V_{//\,plate\,cap.} \cdot q_{acid}}{d \cdot m_{acid}} \tag{6}$$

$$v = \frac{V_{//\,plate\,cap.} \cdot q_{acid}}{d \cdot m_{acid}} \cdot t \tag{7}$$

where $|E|$ is electric field strength, q is electric charge, ε_0 is the permittivity of free space, A is the area of each capacitor plate, V is the voltage across the capacitor, d is the distance between the capacitor plates, F is the force generated, a is acceleration, m is the mass of the particle, t is the amount of time the ion is exposed to the field, and v is the velocity of the particle.

Unlike free space, the acceleration, and therefore the velocity, of an acid ion traveling through a medium such as photoresist is hindered, and so its behavior with respect to equation 5 is impeded. In addition, the velocity of the acid cannot accelerate perpetually; and so the velocity of the acid quickly equilibrates to a maximum velocity as described by equation 8,

$$v_{drift} = \mu \left| \vec{E} \right| \tag{8}$$

where μ is mobility as defined by the Einstein relationship in equation 9,

$$\mu = \frac{q}{k_B T} D \tag{9}$$

where k_B is the Boltzmann constant, T is the temperature of the system, and D is the acid diffusivity for the particular photoresist.

Equation 10 describes the drift velocity of the acid in terms of film thickness, voltage across the resist, temperature, and the diffusion constant. Equation 11 is derived from equation 10 to define the displacement of the catalyst due to drift.

$$v_{drift} = \frac{q_{acid} V D}{k_B dT} \tag{10}$$

$$L_{Drift} = \frac{q_{acid} V D}{k_B dT}(t) \tag{11}$$

Because there is an acid ion concentration gradient, the movement of the catalyst is influenced by diffusion. Fick's second law, listed as equation 12, is used to incorporate diffusion into the model. The acid concentration is represented by φ.

$$\frac{\partial \varphi}{\partial t} = D \frac{\partial^2 \varphi}{\partial x^2} \tag{12}$$

The general solution to the differential equation (Fick's second law) is given in equation 13.

$$\varphi(x,t) = \frac{A}{\sqrt{4\pi Dt}} \exp\left(-\frac{x^2}{4Dt}\right) \tag{13}$$

The diffusion length is the value of x that results in an exponent value of -1; this is the distance the acid travels without an applied electric field, or perpendicular to the

direction of the electric field. For this application, the diffusion length, described in equation 14, is the horizontal acid displacement.

$$L_{Diff} = \sqrt{4Dt} \tag{14}$$

The distance an acid ion moves in the direction of the electric field is governed by both diffusion and drift behavior. Equation 15, which is the summation of equations 11 and 14, can be used to calculate the vertical ion displacement.

$$L_{Drift+Diff} = \frac{q|\vec{E}|D}{k_B T}(t) + \sqrt{4Dt} \tag{15}$$

Equation 16 describes the vertical displacement of the acid in terms of film thickness, voltage across the resist, temperature, and the diffusion constant.

$$L_{Drift+Diff} = \frac{q_{acid}VD}{k_B dT}(t) + \sqrt{4Dt} \tag{16}$$

Because of acid-to-acid electrostatic interaction, an electrostatic force will cause the ions to move away from each other in the same manner as diffusion. This force can be neglected for low catalyst concentrations.

Mosong Cheng and Andrew Neureuther, in their 2003 publication in the Journal of Vacuum Science and Technology [7], reference a measured range of DUV CAR acid diffusivity of between 10^{-7} and 10^{-3} $\mu m^2/s$ and used a value of 9×10^{-6} $\mu m^2/s$ for their mathematical modeling of acid displacement in Shipley UVIIHS.

Equation 17 relates the acid concentration with respect to the initial photoacid generator (PAG) concentration in terms of α, which is the quantum yield of acid generation (the Prolith parameter is called the acid generation coefficient), and E, the exposure dose [13].

$$\frac{\left[H^+ \right]}{\left[PAG \right]_0} = 1 - e^{-\alpha E} \tag{17}$$

The PAG concentration is typically about 2 mol % of the photoresist. Using Rohm and Haas UV6 positive DUV photoresist as an example, the quantum yield of acid generation is measured at 0.051 cm^2/mJ and the exposure dose-to-size is between 18.0 and 28.0 mJ/cm^2 [14]. Under these conditions, the acid concentration would be between 1.2 and 1.52 %, which is a significant enough percentage that an attempt should be made to describe this behavior, although detailed models will not be developed at this time.

The electric field strength at any point away from the surface of an infinite sheet with a volume charge density ρ and thickness s is given by equation 18. It is assumed that the charge is evenly distributed.

$$E_{\infty\, sheet} = \frac{\rho}{2\varepsilon_0}(s) \tag{18}$$

Treating the exposed volume of photoresist as an infinitely long space with an infinitely large aspect ratio, equation 19,

$$E_{H^+ to\, H^+} = \frac{\rho}{\varepsilon_0}(x) \tag{19}$$

where x is the distance away from the center of the exposed region of the photoresist, can be used to calculate the strength of the electric field at any position within the exposed portion of the photoresist that is a significant distance away from the silicon interface. The electrostatic effect of adjacent exposed regions is neglected. Notice that a position centered in the exposed resist is not subject to an additional electric field, and a position at the edge of the exposed region, that is, $x = (s)/2$, is subject to the same electric field

described in equation 18. It is important to state that the exposed width is a function of time, as it will change due to diffusion and acid-to-acid electrostatic force.

Again applying equations 4 and 8 to this new circumstance, equation 20 describes the velocity resulting from acid-to-acid electrostatic force. This factor can be added to equations 12 and 14.

$$v_{H^+ to H^+} = \mu \frac{\rho}{\varepsilon_0}(x) \tag{20}$$

Comparing equation 14 with equation 16, it can be determined that if the temperature and time of the post exposure bake are reduced, and an electric field is induced, the lateral diffusion length of the acid catalyst will decrease, and the vertical diffusion length will increase. Acid catalyst movement due to acid-to-acid electrostatic interaction can only be decreased with a reduction of the PEB time.

2.3 Applied Theory

With a process-defined photoresist thickness determining the electrode distance, the photoresist chemical formulation determining the PEB temperature, and the available power supply determining the electrical potential, the remaining variables to be optimized are the applied voltage frequency and EFE-PEB time. To characterize the effect of these two factors, equations 11, 14, and 16 are plotted with respect to PEB time in Fig. 2.2 using appropriate values for the previously defined variables. The calculations will use the same diffusivity value for Shipley UVIII as Mosong Cheng and Andrew Neureuther used for Shipley UVIIHS. This is a reasonable assumption because the two resists are similar enough to share select information on the UVIII datasheet [3].

18

Acid Catalyst Drift & Diffusion Length vs. Post Exposure Bake Time for a 5V 130°C EFE-PEB Across 0.4µm of Photoresist

$$L_{Diffusion} = \sqrt{4Dt}$$

$$L_{Drift} = \frac{q_{acid}VD}{k_B dT}t$$

Legend:
- —○— Diffusion Length
- —□— Drift Length
- —△— Total Acid Displacement

X-axis: PEB Time [s]
Y-axis: Drift & Diffusion Length [nm]
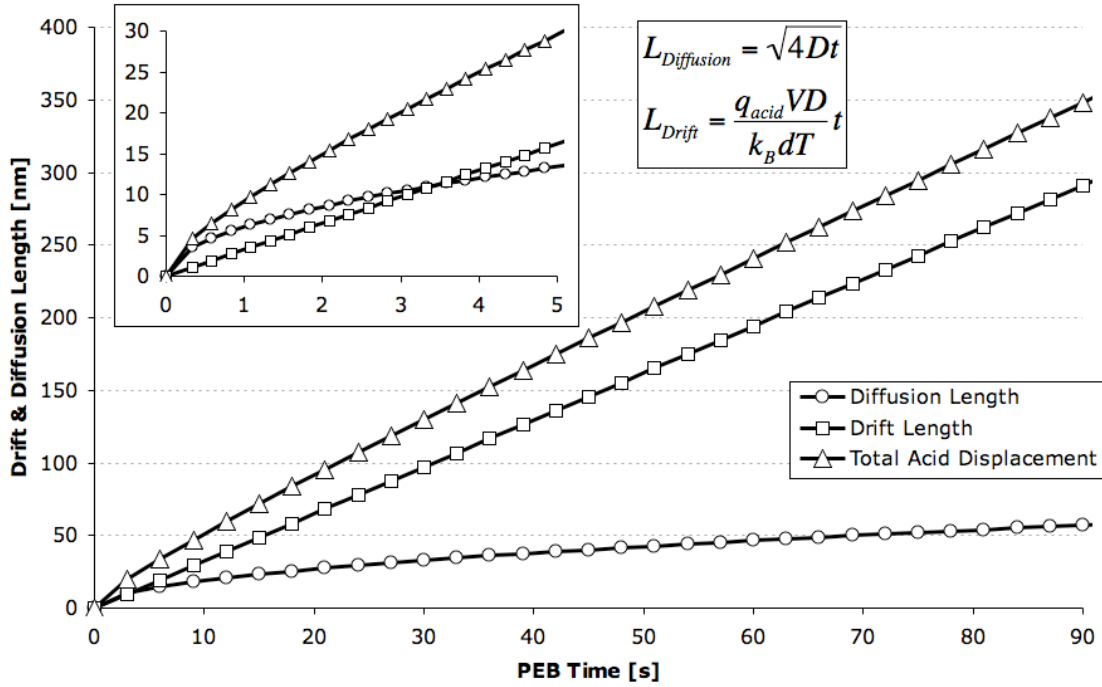
Fig. 2.2. Acid displacement due to drift and diffusion.

Any process enhancement offered by EFE-PEB over a PEB can be observed experimentally by comparing thickness loss, which is a function of diffusion length, between areas receiving either EFE-PEB or PEB. This can be done with equal bake times and different diffusion lengths showing enhanced thickness loss, or with different bake times and equal diffusion lengths showing equal thickness loss.

Chapter 3

Experimental Methods, Data, and Analysis

3.1 Principal Experimental Procedure

In order to generate the electric field of the design described in the theory section, two electrodes are placed on either side of the sample wafer coated with photoresist. The hotplate used to deliver the PEB is a natural choice for the bottom electrode; a highly doped, and therefore conductive, wafer will effectively extend the bottom electrode to the silicon-photoresist interface. The top electrode is manufactured by depositing aluminum on an insulation layer grown or deposited on a silicon wafer and is placed in contact or near-contact with the photoresist during the PEB.

The wafers used for this project are 150 mm in diameter, 0.625 mm thick, and are doped n-type with arsenic to a sheet resistance between 0.0015 Ω/square and 0.0040 Ω/square. Prior to photoresist application, wafers undergo a dehydration bake at 150°C for 60 seconds. Shipley UVIII positive DUV photoresist is spin coated by hand before receiving a 60 second softbake at 130°C to planarize the film and evaporate excess solvent. The sample is exposed to DUV radiation through a 254 nm wavelength filter via a fluorescent lamp that operates at 120 V, 0.7 A, and 60 Hz. The DUV lamp contains no homogenizing optics and is operated manually with an on/off switch. A voltage source is used to apply an electric potential between the top electrode and hotplate during a 90 second long 130°C PEB. After cooling on a metal plate for 15 seconds, the wafer is submerged in CD-26, a 0.26 N tetramethylammonium hydroxide (TMAH) developer, which has been diluted 50% by volume with deionized (DI) water. After 20 seconds in

the developer, the wafer is immediately submerged in DI-water to terminate the development. The wafer is blown dry with compressed air before undergoing metrology.

The developer is diluted to reduce the contrast and increase the dose-to-clear of the photoresist; this increases the range of exposure doses that result in thickness loss and reduces the effects of changes in radiation intensity on development rate. Using 150 mL developer to 150 mL DI-water, the development rate is noticeably reduced after 6 wafers have been processed; to avoid wafer-to-wafer variation, the wet chemistry is replaced after every 4 runs.

For baseline data, wafers were flood exposed, underwent a PEB, and developed in the developer solution as previously described. Because the lamp consists of two fluorescent bulbs behind a 254 nm filter, the exposed region was in the shape of two parallel ovals, with one experiencing more thickness loss than the other, ostensibly due to a difference in irradiance between the two bulbs. The resist exhibited significant thin-film interference around the cleared regions, which could be caused by the diluted developer reducing the contrast.

3.2   Preparatory Attempts: Uniform Electric Field

These preliminary experiments used a top electrode manufactured by evaporating 3000 Å of aluminum on a silicon wafer with 1.5 μm of TEOS deposited by PECVD. No features were etched into the conductive film; this results in an uninterrupted, uniform, and parallel electric field between the top electrode and hotplate. The top electrode wafer was cleaved into two equal pieces and constructed into an apparatus that delivers an electric field over half of the surface of an exposed wafer during the PEB. The half-wafer

was attached to a stack of 2 other wafer pieces so that it could straddle over the sample and was connected via an alligator clip to ground while the hotplate was connected to a positive DC voltage; in this manner, 63 V were applied across the sample with the field emanating from the silicon/resist interface and pointing towards the top electrode.

The photoresist was coated to a thickness of just under 0.6 μm. Flood exposures were conducted with the wafer 4 cm below the DUV lamp. The desired exposure time was determined by exposing 4 divisions of one wafer, defined by the edge of a metal foil, for a progressively increasing amount of time.

For the first experiment, an electrically floating control top electrode was partially wrapped in Teflon tape and placed on the surface of the sample wafer; this setup is shown in Fig. 3.1. After following the procedure outlined in section 3.1, visual inspection revealed a thickness loss enhancement on the side of the sample that received an EFE-PEB.

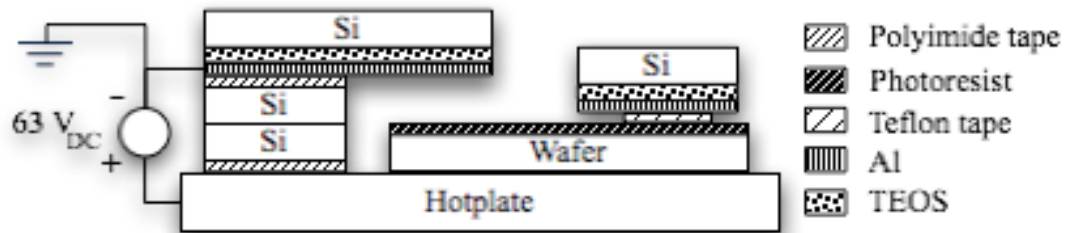Fig. 3.1. Diagram of EFE-PEB test setup using Teflon tape to separate the electrically floating control top electrode from the photoresist. Not drawn to scale.

Because the Teflon tape is significantly thinner than one wafer thickness, the top electrode was positioned further away from the sample than the control electrode. This could cause an increased amount of base contamination on the control side, which would

22

inhibit photoresist development and account for the observed thickness loss enhancement. To make any contamination effects even between the control and experimental sides of the sample, the control was modified to rest on silicon wafer pieces one wafer thick; as shown in Fig. 3.2, this results in very similar spacing.
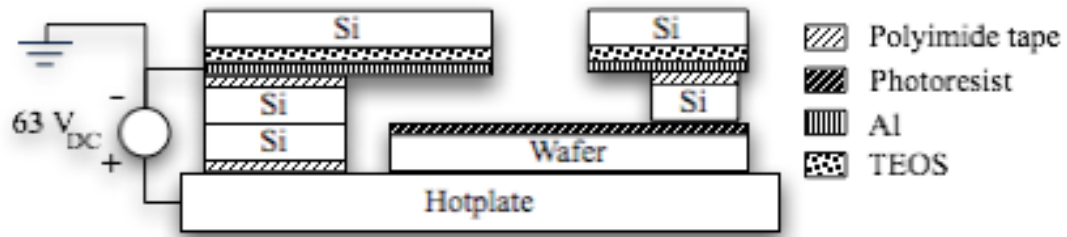
Fig. 3.2. Diagram of EFE-PEB test setup using a wafer piece and polyimide tape to separate the electrically floating control top electrode from the photoresist by the same distance as the experimental top electrode. Not drawn to scale.

The first experiment under the new conditions resulted in no observable thickness loss enhancement on the EFE-PEB side of the sample. It was discovered that the polyimide tape used to secure the control electrode to the silicon wafer pieces separating it from the photoresist was looped in such a way as to raise the control electrode an additional couple of millimeters above the surface of the sample. Again attributing changes in resist thickness loss to base contamination, the control setup was altered to provide a more intimate contact between the control electrode and the supporting wafer pieces. This new arrangement resulted in a thickness loss enhancement of 1320 Å, as measured by spectroscopic reflectometry, on the EFE-PEB side of the sample.

Subsequent attempts to reproduce the results consecutively were unsuccessful. Flood exposures with a PEB were employed as a diagnosis tool, and it was found that the

spatial distribution of the intensity of the lamp changes over time; what would appear to be an oval-shaped field in one exposure would develop into a peanut-shaped field in a later one. This characteristic of the radiation source prevents repeatability of the experiments and reduces confidence that the control and experimental regions of the photoresist receive equal doses.

In an effort to reduce the effects of the intensity variation so as to deliver an equal dose to both halves of the wafer, a small area of the lamp filter was portioned off with metal foil. The resist-coated wafer was placed in contact with the foil, and by swiftly moving the wafer in a step-and-repeat behavior over the uncovered portion of the filter, two equal sized dies were exposed that correspond in their position with the EFE-PEB and control positions of the experimental setup. However, since exposure time was controlled by hand, satisfactorily equal doses could not be delivered to each die.

3.3   Preparatory Attempts: Spatially Periodic Electric Field

Although the radiation intensity from the lamp changes spatially over time, it can be reasonably assumed that areas in close proximity receive equal exposure doses. Therefore, if both EFE-PEB and PEB experiments can be administered over a small area, their exposure conditions can be said to be equivalent. To implement this setup, a top electrode was fabricated by sputtering 200 Å of aluminum on a silicon wafer with 1.5 μm of TEOS deposited by PECVD. A 10 μm pitch pattern of equal lines and spaces was lithographically defined via contact printing and the pattern was transferred into the aluminum film with a wet etch. The pattern covered a majority of the wafer's surface with a remaining aluminum border for contact with the voltage source alligator clips.

Applying a voltage between the aluminum lines and the wafer will provide successive iterations of regions receiving field enhancement and regions serving as a PEB control over any small region of the exposed photoresist.

To reduce wafer-to-wafer exposure variation, the lamp was allowed to warm up for 5 minutes before exposure. After exposure, it was left off for 10 minutes to cool. Consecutive control flood exposures appeared similar after development under these conditions.

The desired dose would be sub-clearing and would result in significant thickness loss. This is undemanding because the unhomogenized optics and diluted resist developer provide gradual thickness loss variation across the wafer; there is a broad range of exposure times that provide the desired result.

After exposure, the patterned top electrode was placed with the aluminum features in contact with the resist. The assembly was placed on a hotplate and a 63 V bias was applied to the hotplate, which was grounded, and top electrode, which had a negative bias, during a 130°C PEB. After 90 seconds, the voltage source was switched off, the top electrode was removed, and the wafer was placed on a cooling plate for 15 seconds before being developed for 20 seconds in the diluted TMAH solution.

Initial results showed an increase in contrast. The regions that had developed away had an abrupt transition from clearing dose to unexposed, with spotted remnants of resist remaining in the cleared area. With repetition, this effect gradually reduced in severity and the photoresist eventually resembled the control. It is surmised that base contamination from the top electrode was neutralizing the acid catalyst, and that repeated bakes in contact with the photoresist reduced the contamination levels.

Upon examination of the developed wafer under profilometry around areas of resist in which the remaining thickness transitioned between about 1650 Å and 750 Å, 2 visually rough-looking patches measured a subtle thickness loss enhancement of about 50 and 70 Å that repeated every 10 μm. The profilometry measurements are shown in Fig. 3.3 and Fig. 3.4.

For more accurate measurements, the sample was inspected via AFM. Under the optical microscope of the AFM, apparent scratches were found that were composed of 10 μm pitch repeating lines and spaces. The line of features faded to pinholes at either end while maintaining a 10 μm pitch before terminating. The profile of one such observed scratch with an 86 nm step height is shown in Fig. 3.5. The wafer was placed on an optical microscope and micrographs were taken of the scratch, which are shown in Fig. 3.6.
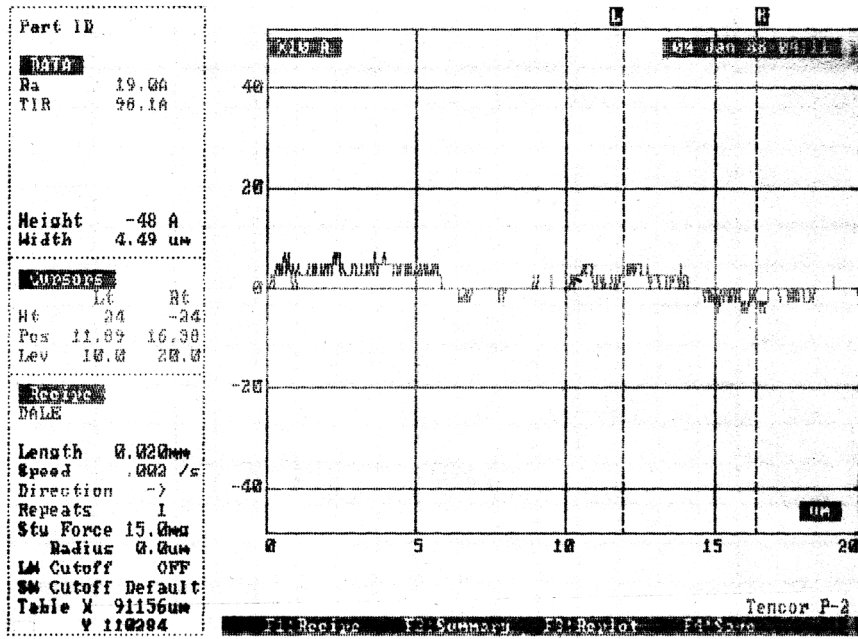
Fig. 3.3. Profilometry measurement of the rough-looking area of the photoresist measuring a 48 Å periodic thickness loss enhancement repeating every 10 µm. The EFE-PEB was applied using a silicon wafer with 10 µm pitch aluminum lines and spaces on TEOS as a top electrode.
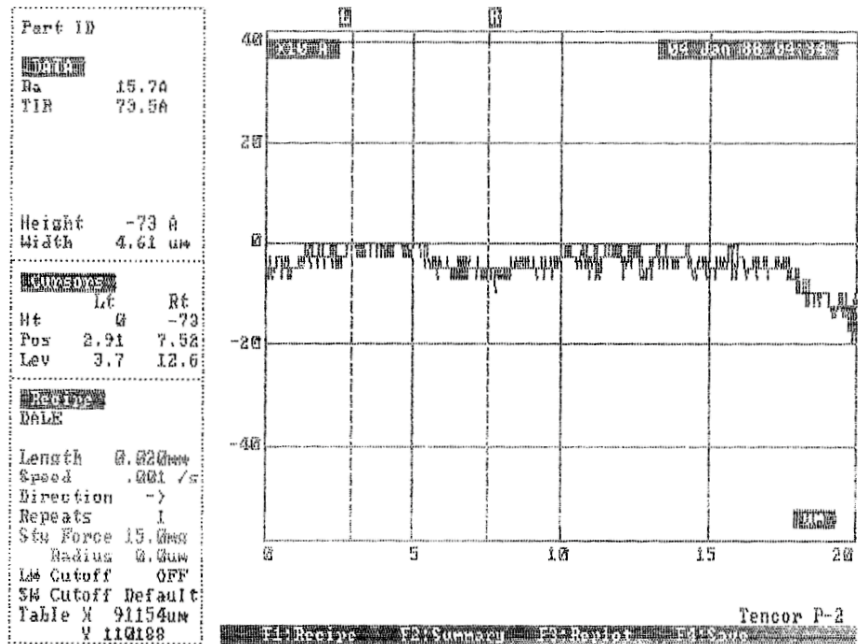
Fig. 3.4. Profilometry measurement of the rough-looking area of the photoresist measuring a 73 Å periodic thickness loss enhancement repeating every 10 µm. The EFE-PEB was applied using a silicon wafer with 10 µm pitch aluminum lines and spaces on TEOS as a top electrode.

Fig. 3.5. Cross section of repeating regions of thickness loss enhancement, appearing as 10 μm pitch scratches with an 86 nm step height, as measured using AFM.
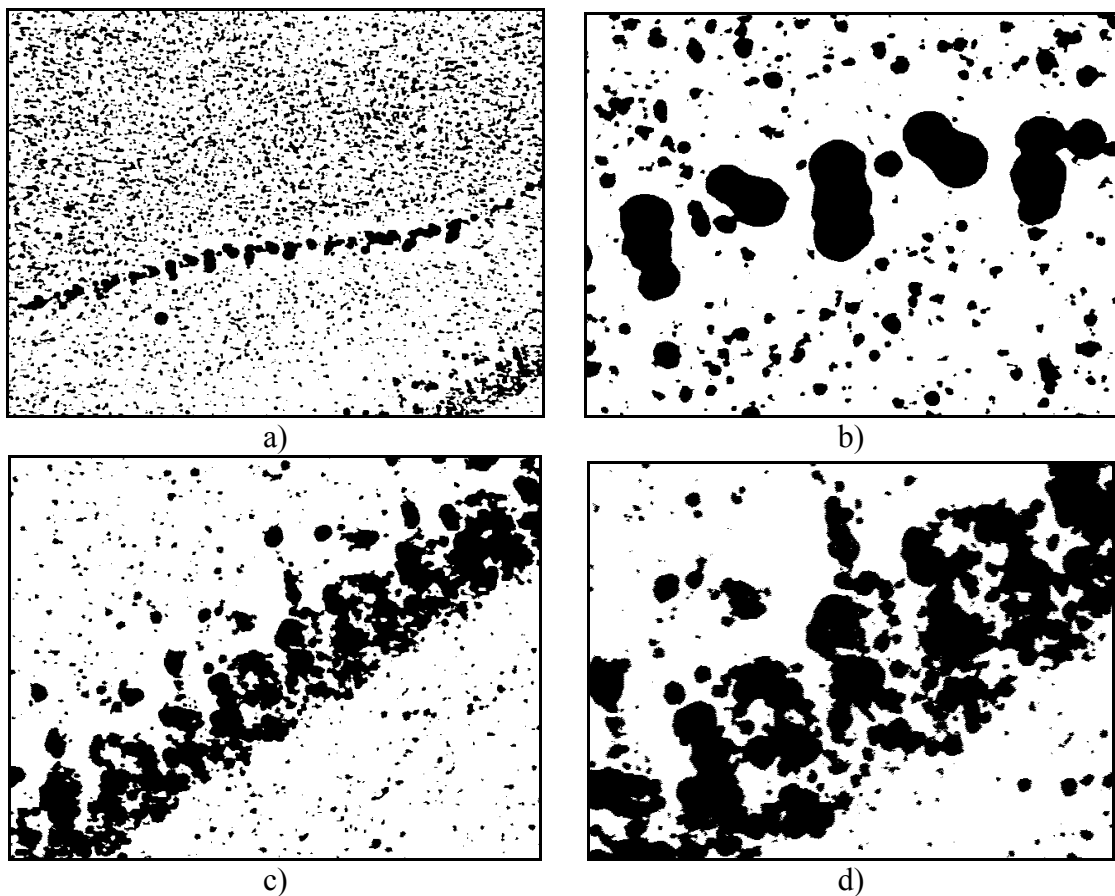
Fig. 3.6. Optical microscope image captures, altered to black and white, of 2 different scratches consisting of periodic features that repeat every 10 μm. The first location, which is the feature inspected via AFM, is shown at a) 200x and b) 1000x magnification. The second location is shown at c) 500x and d) 1000x magnification.

28

The repeating features resolved in the resist were of an inconsistent form and extended in only one direction. It was hypothesized that if electrical contact was being made to the backside of the wafer the contrast in field strength between EFE-PEB and PEB regions would be diminished, making distinction between the two more subtle. Also, surface roughness between the resist and top electrode would decrease the effectiveness of the electric field in enhancing the acid displacement in areas separated from the top electrode. Inspecting the EFE-PEB setup with a voltmeter, it was found that there is both a 63 V potential between the backside of the wafer and the hotplate and between the aluminum lines and the hotplate. The front side of the wafer was insulated from the aluminum features with PECVD TEOS, but this did not insulate the backside of the highly doped wafer from the voltage source's alligator clips.

A solution to the backside contact problem was found in the quartz mask used to image the aluminum features on the silicon wafer top electrode. The chrome lines of the mask served as a conductor with patterned features identical to those imaged on the silicon electrode, and the quartz substrate served as the electrical insulator.

The procedure was repeated using the quartz mask as a 10 µm pitch top electrode in the wafer's stead. Again, the initial exposures were developed with a resulting spotted appearance and high contrast. This subsided with repetition as it did with the wafer as top electrode.

The photoresist thickness was reduced to 0.4 µm by increasing the casting spin speed from 1500 RPM to 3000 RPM to increase the strength of the electric field by reducing the distance between the electrodes in an effort to make any field enhancement

more prominent. The procedure was again repeated with the quartz mask as the top electrode and the exposed wafer was inspected on the profilometer. Measuring areas of resist that looked similarly rough to the previous profilometry measurements, surface topology repeating every 10 μm, shown in Fig. 3.7, was found suggesting a thickness loss enhancement of about 120 Å.
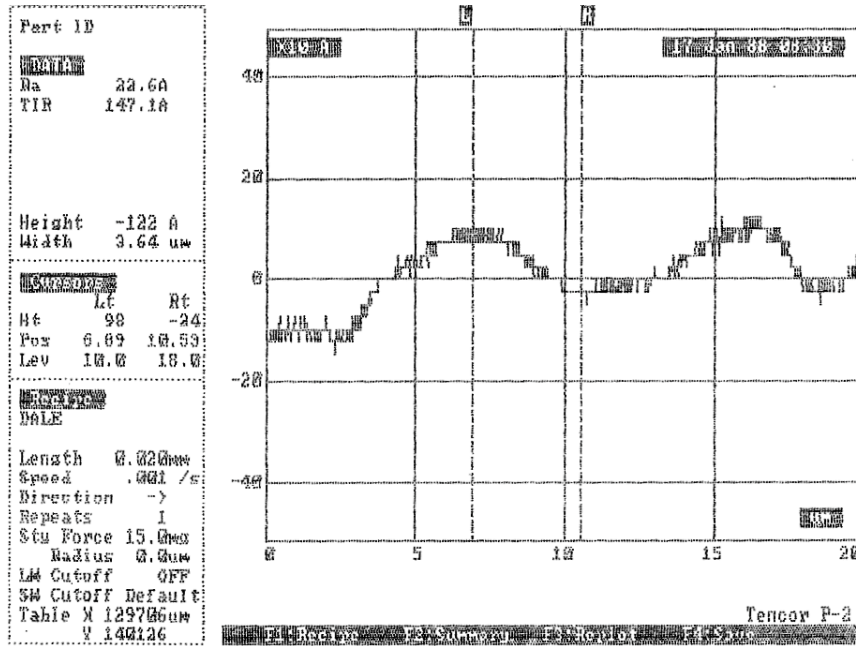
Fig. 3.7. Profilometry measurement of the rough-looking area of the photoresist measuring a 122 Å periodic thickness loss enhancement repeating every 10 μm. The EFE-PEB was applied using the quartz mask top electrode.

Although the measured periodic thickness loss enhancement had increased with a shorter electrode separation and better electric field contrast, the areas of developed photoresist exhibiting field enhancement were still small compared to the area over which the alternating zones of PEB and EFE-PEB were being applied. To address this inconsistency, the sample size was reduced to limit the influence of surface roughness and attention was returned to the theory in order to optimize field effects.

3.4 Alternating Voltage Polarity Experiments

The previous experiments were conducted with the highest DC voltage the power source could provide. It is possible that the acid catalyst was simply being forced to the interface and pinned in a stationary position, which would prevent deprotection. Section 2.3 outlined the consequences of specific variables on the acid displacement and Fig. 2.2, which plots the kinetic behavior of the catalyst under PEB and EFE-PEB, can be used to predict the consequences of a designed experiment.

The first such experiment used the quartz mask with 10 μm pitch equal lines and spaces as the top electrode and the same parameters as those used to create Fig. 2.2. Looking at this figure, the acid diffusion length at 90 seconds is about the same as the total acid displacement at 12.5 seconds, and about half of the total acid displacement at 25 seconds. This means that a square wave with a frequency of 0.02 Hz would double the acid displacement between EFE-PEB and PEB. Because the plot uses a 5 V_{DC}, the experiment will swing between +5 and -5 V. To address the problem of limited surface area exhibiting field enhancement, which was thought to be caused by surface roughness and coating inconsistencies, smaller samples were used and pressure was applied to increase contact between the resist and top electrode. This was achieved by cleaving the photoresist coated wafer into 1.5 cm by 7 cm pieces and placing a Pyrex dish atop the patterned electrode. Curiously, no periodic thickness loss enhancement was observed under profilometry after development.

Up until this point, the number of acid catalyst molecules has been assumed to remain constant over the PEB time, but the previous results suggest otherwise. Electrons

injected into the photoresist from the cathode is a possible mechanism for acid neutralization. As was done with the top electrode in [7] and [9], an acid diffusion insulation layer must be applied to the electrodes before resist processing.

The material used as an acid diffusion barrier in the aforementioned papers was a hardbaked i-line photoresist. In this case, the resist will be OiR 620. To facilitate spin coating a thin film on the top electrode, a new 150 mm wafer-based design was manufactured to replace the quartz mask. This was done by sputter depositing 4500 Å of aluminum on a 5000 Å thick thermally grown silicon dioxide layer. A pattern of 10 μm pitch equal lines and spaces was defined with proximity lithography and a wet chemical etch using the same quartz mask the new electrode was meant to replace. The thin and round wafer substrate is easier to spin coat than the thick square quartz mask, and the thermally grown oxide electrically insulates the backside from the alligator clips connected to the voltage source.

After the top electrode wafer underwent a dehydration bake, the OiR 620 was applied and underwent a standard bake processes on an SSI wafer track. The diffusion barrier was spin coated at 3250 RPM for 30 seconds and softbaked at 90°C for 60 seconds. Skipping exposure and development, the wafer was baked at 110°C for 60 seconds, which would have been the PEB, and was hardbaked at 140°C for 60 seconds. A blank silicon wafer receiving identical process steps was left with a resist layer averaging 9630 Å thick as measured by spectroscopic reflectometry. An edge of the aluminum border left by the quartz mask was exposed by etching away the covering photoresist with acetone. This final step allows electrical contact between the alligator clips and aluminum features.

The exposure, EFE-PEB, and develop procedure was repeated with the new patterned top electrode. Pressure was not applied because the silicon wafer substrate is more fragile than the thicker quartz mask. Five samples each of two different film stacks were processed—one with CAR coated directly on silicon, and one with CAR coated on another hardbaked i-line resist layer that was deposited with the same process as was used to coat the top electrode. Equations 11, 14, and 16 were again used to optimize the square wave frequency, this time swinging between +10 V and -10 V, so that the catalyst displacement would be double the diffusion length achieved by PEB. This resulted in 25 mHz being used for the 1360 nm electrode spacing, which is defined by the top electrode acid diffusion barrier and CAR thicknesses, and 16 mHz being used for the 2320 nm electrode spacing, which is defined by the top electrode acid diffusion barrier, bottom acid diffusion barrier, and CAR thicknesses. For the case of the 2320 nm electrode spacing samples, the CAR thickness was assumed to be 0.4 μm.

After development, the 10 samples were inspected via profilometry. None of the samples containing a bottom acid diffusion barrier exhibited periodic thickness loss. It is likely that the thickness assumption was incorrect, which resulted in an un-optimized frequency calculation. A single sample baked with an electrode distance of 1360 nm exhibited a periodic topology repeating every 10 μm. Measurements were taken at a location adjacent to a cleared region of photoresist, and are shown in Fig. 3.8 and, along a broader measurement range, Fig. 3.9. Again, such results were only obtained from areas that looked rough under the microscope in the profilometer.
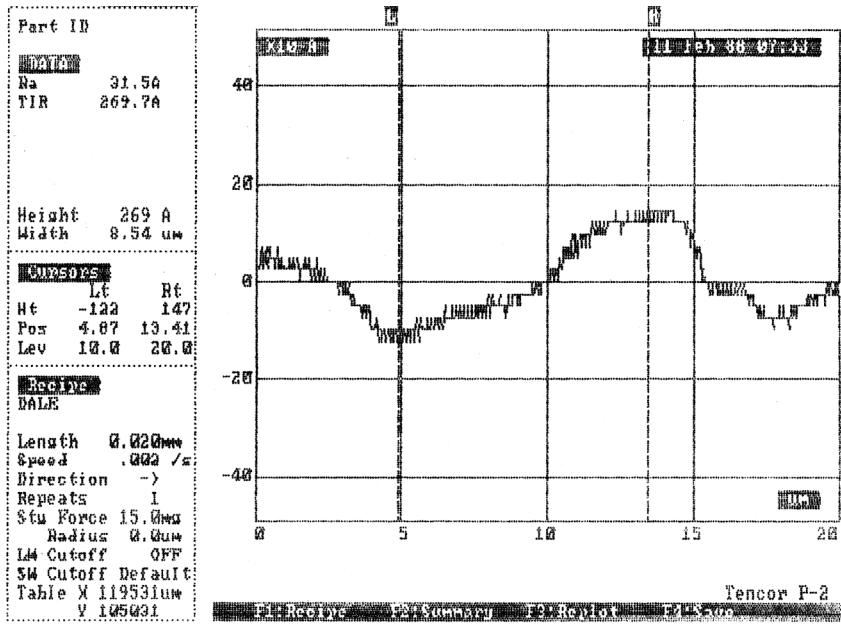
Fig. 3.8. Profilometry measurement of the rough-looking area of the photoresist measuring a 269 Å periodic thickness loss enhancement repeating every 10 µm. The EFE-PEB was applied using a silicon wafer with 10 µm pitch aluminum lines and spaces on thermal oxide as a top electrode. The electrode was coated with an acid diffusion barrier.
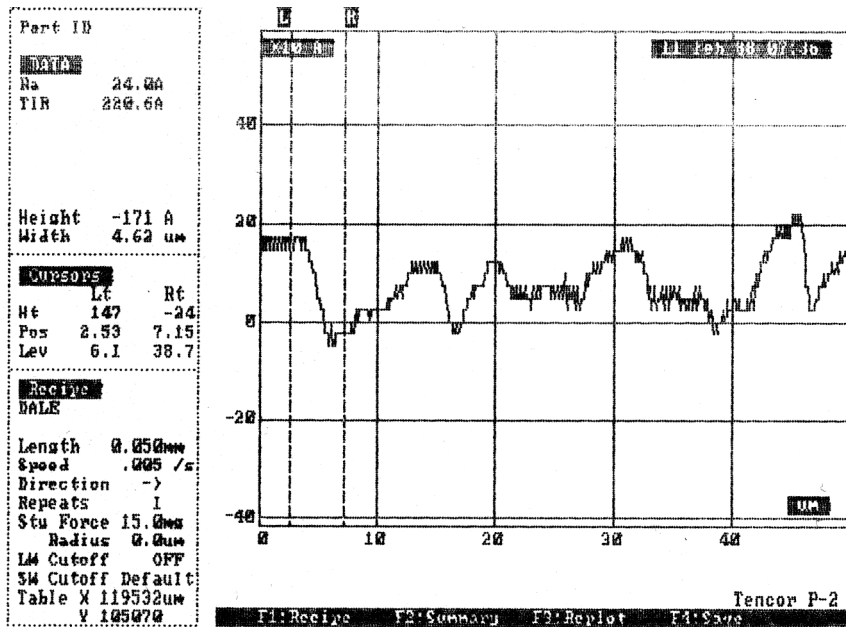
Fig. 3.9. Profilometry measurement, repeated at the same location as Fig. 3.8, taken over an expanded range. Across 50 µm, 5 peaks and 5 valleys are visible indicating a 10 µm pitch over the entire measurement space.

AFM inspection of the wafer sample did not yield similar results to the profilometry data. In addition, what is considered to be the source of the rough-looking topology was discovered to be a layer of photoresist folded over itself. A screen capture of the AFM's optical microscope is shown in Fig. 3.10. In the image, crosshairs are placed over bare silicon. The darker portion of photoresist, shown in the upper right hand corner of the image, has a flat interface with the bare silicon, which is at the bottom of the image; the straight line separating the regions suggests a fold. In addition, the jagged border between the darker and lighter resist regions is the mirror image of the border between the lighter resist and bare silicon.
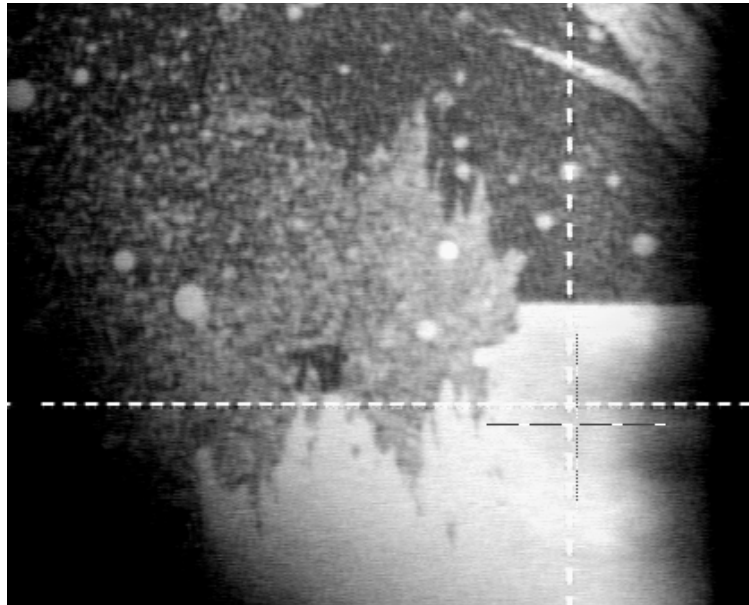
Fig. 3.10. Optical micrograph taken from the AFM of a fold in the DUV photoresist.

This observation suggests what was considered to be a periodic thickness loss may in fact be ripples caused by an unrelated mechanism such as adhesion failure. In view of the scarce realization of locations exhibiting surface roughness, concern over the data's cogency extends to the previous experiments.

Chapter 4

Failure Analysis

Before the discovery of folded photoresist, the data suggested an increase in thickness loss enhancement with each progressive step of the experimental design's evolution—a trend suggesting support for the theory. Table II lists each design and the corresponding thickness loss enhancement as measured by profilometry. However, the observed fold puts into perspective the localization of periodic thickness loss to regions of exposed photoresist immediately adjacent to areas receiving a clearing dose. Therefore to maintain comprehensive standards it is appropriate to investigate possible failure modes.

TABLE 4.1

SUMMARY OF EXPERIMENTAL DESIGN AND PROFILOMETRY DATA

Exp.	Purpose	Setup	Δt_{loss}
1	Initial experimental design	Uniform E-field pointing up 63 Vdc, 0.6 μm PR thickness	0 Å
2 a	Remove lamp variability over data collection area	10 μm pitch top electrode 　(TEOS wafer) 63 Vdc, field pointing up 0.6 μm PR thickness	50 Å, 70 Å
2 b	Increase experimental E-field strength, remove control E-field	10 μm pitch top electrode 　(quartz mask) 63 Vdc, field pointing up No backside contact 0.4 μm PR thickness	120 Å
3 a	Increase electrode contact area, reduce acid pileup at electrode/PR interface	10 μm pitch top electrode 　(quartz mask) ±5 V, 0.02 Hz square wave 　(double PEB acid displacement) No backside contact 0.4 μm PR thickness 1.5x7cm sample Pressure on electrode into PR	0 Å
3 b	Decrease acid neutralization at the cathode	10 μm pitch top electrode w/ acid barrier 　(thermal oxide wafer) Acid barrier at PR/wafer interface ±10 V, 0.016 Hz square wave 　(double PEB acid displacement) No backside contact 0.4 μm PR thickness 1.5x7cm sample	0 Å
3 c	Decrease acid neutralization at the cathode	10 μm pitch top electrode w/ acid barrier 　(thermal oxide wafer) ±10 V, 0.025 Hz square wave 　(double PEB acid displacement) No backside contact 0.4 μm PR thickness 1.5x7cm sample	270 Å

4.1   Review and Test of Assumptions

Each of the experiments listed in Table II share three assumptions: the number of acid molecules is constant, an electric field is present in the experimental partition of the photoresist, and no electric field exists in the control. The amount of acid in the resist would decrease under conditions enabling charge exchange between the resist and electrodes; new theory would have to be applied to predict the consequences of such an environment, as it is conceivable that a changing acid level could both inhibit thickness loss by reducing the number of catalyst molecules and enhance thickness loss by preventing pileup at the electrode interface and reducing coulomb repulsion. If an electric field either does not exist in the experimental region, or does exist in the control region, conditions between the two will be identical, and therefore no thickness loss enhancement would be observed.

To test both experimental and control sections for the presence of an electric field, a bias was placed across the hotplate and patterned top electrode while a multimeter measured current between the two. A current was observed through the multimeter while probing the hotplate and aluminum lines on the top electrode; this supports the assumption that a field exists in the photoresist intended to receive an EFE-PEB. After moving the top electrode multimeter probe from the aluminum lines to an area of exposed oxide, no current was observed. However, should electrical contact be made to the top electrode substrate, a weaker field would still be present in the control. To test for this condition, hydrofluoric acid was used to etch away an area of oxide on the backside of the wafer so that electrical contact could be made to the substrate with a multimeter

probe. Again applying a bias across the hotplate and aluminum features on the top electrode, an electric current was measured from the electrode substrate through the multimeter to the hotplate. This suggests that the aluminum features are shorted to the substrate and the assumption of no electric field in the control is violated.

To test the first of the three assumptions—that the number of acid molecules does not vary with time—an experiment was run repeating the EFE-PEB setup used in experiment 2 b, as denoted in Table II, using 1.5 cm by 7 cm wafer samples while measuring current across the two electrodes. Current was measured over an 18 minute EFE-PEB using 5 samples each of 3 different exposure levels. The unexposed treatment combination serves as a control, having no photogenerated acid. Initially, pressure was applied to the top electrode by placing a Pyrex dish atop the experimental setup, as was performed in experiment 3 a; this caused an electrical short through the photoresist so the experiment proceeded sans pressure.

Because a DC voltage was being applied, if electrons from the cathode are neutralizing photogenerated acid, the plot of current vs. time would be expected to decrease as the EFE-PEB progresses until all of the acid is neutralized and the current stabilizes at the level resulting from electrons drifting from the cathode to the anode. The resulting data is plotted in Fig. 4.1 in its entirety.

Current Across UVIII vs. Time
(-63 Vdc Top Electrode, GND Hotplate)
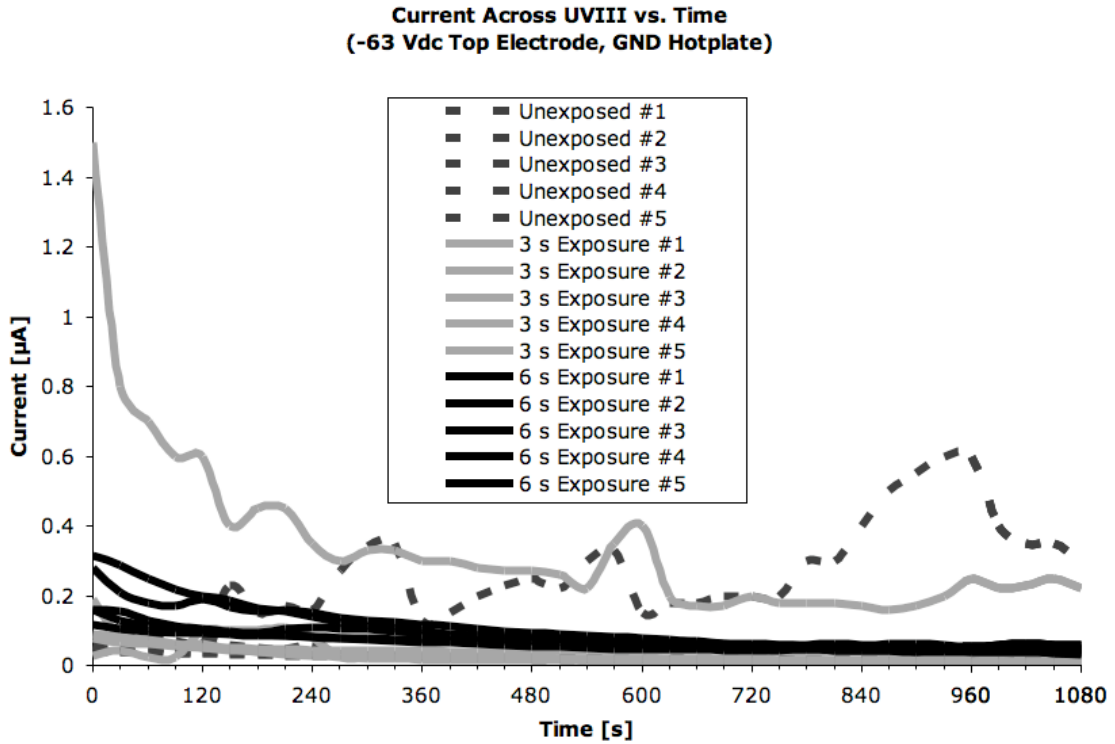
Fig. 4.1. Unedited data generated by the ion current experiment.

Two datasets from the ion current experiment stand out as having significantly larger values than those found in the comparable treatment combinations. These are thought to be shorts and their exclusion results in Fig. 4.2. The averages of the datasets are plotted in Fig. 4.3, and the average current difference from the control is plotted in Fig. 4.4; both plots exclude the two shorted datasets.
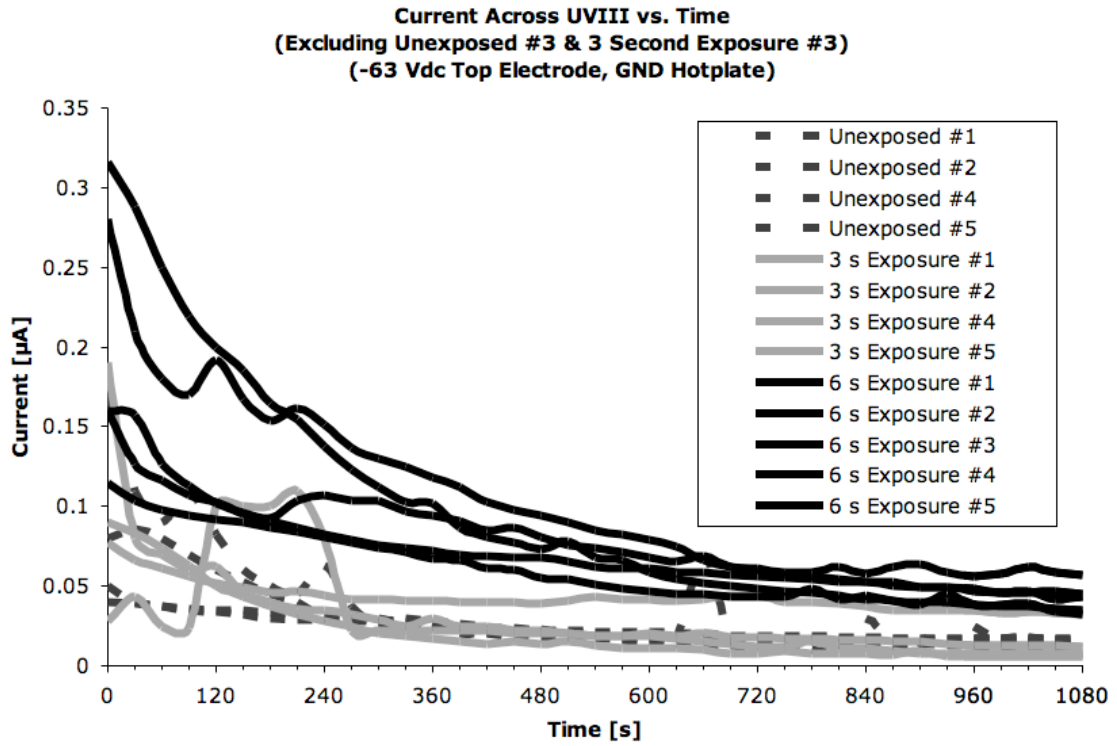
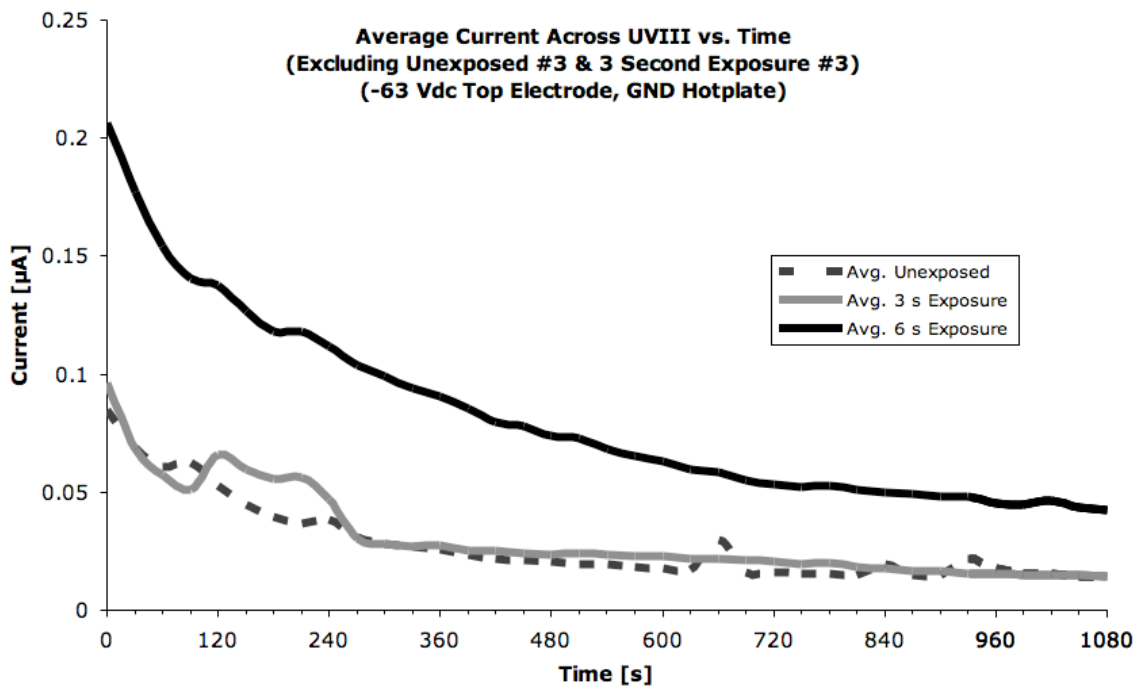Fig. 4.2. Ion current data with shorted datasets excluded.

Fig. 4.3. Average of ion current data with shorted datasets excluded.

41

Fig. 4.3 exhibits the predicted characteristics of the experimental system undergoing acid neutralization from the cathode. The current across the photoresist is at its zenith when the EFE-PEB is initiated and decreases at a continuously decreasing rate as the bake progresses until settling out at a constant value. To investigate how the experimental differs from the control, the data plotted in Fig. 4.3 was calculated in terms of difference from the unexposed dataset; the result is shown in Fig. 4.4.
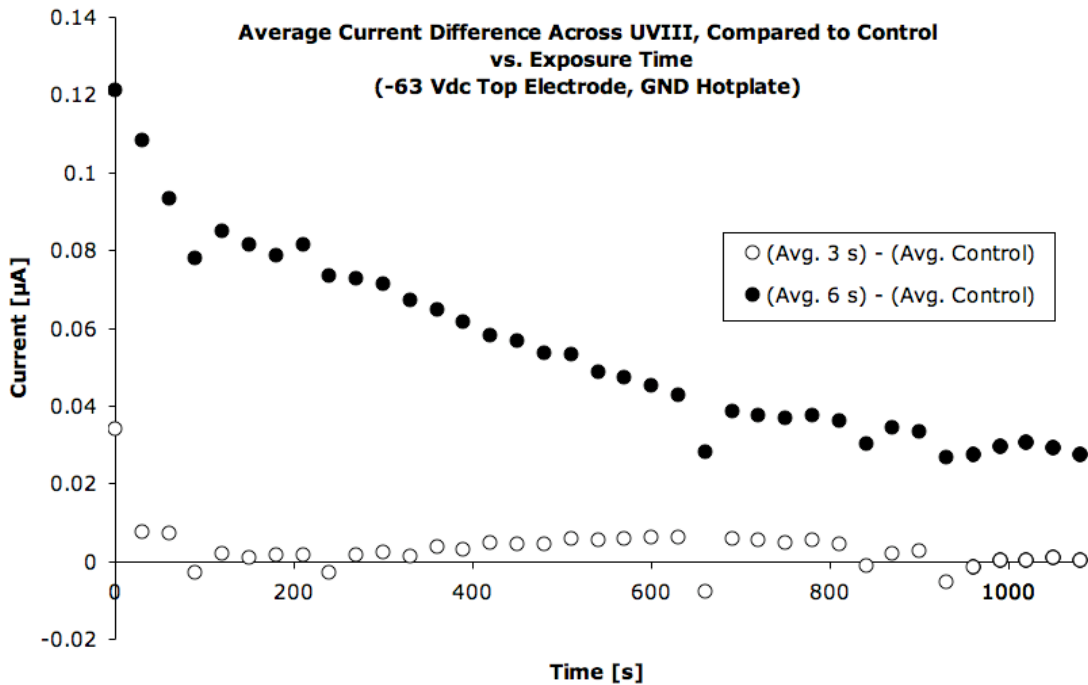
Fig. 4.4. Average ion current data with the control subtracted from the experimental.

Although outliers do exist in the case of a sub-clearing dose, Fig. 4.4 shows that current increases with exposure; this corresponds with an increase in the number of photogenerated charges being moved by the electric field. Current decreases as the acid is neutralized and the number of photogenerated charges falls to zero, at which point the measured current is equal to the electron drift from one electrode to the other. The final

current shown in Fig. 4.3 and Fig. 4.4 differs between the two exposure levels, suggesting that there is a change in conductivity associated with deprotecting the photoresist.

The 6 s exposure dataset, which has the most prominent characteristics and strongest signal in Fig. 4.4 because the 3 s exposure dataset has been starved of charged molecules by quenching agents in the resist, contains three discernable zones within which the current level changes uniformly. The dataset is again plotted in Fig. 4.5 overlaid by three lines approximating the zones.
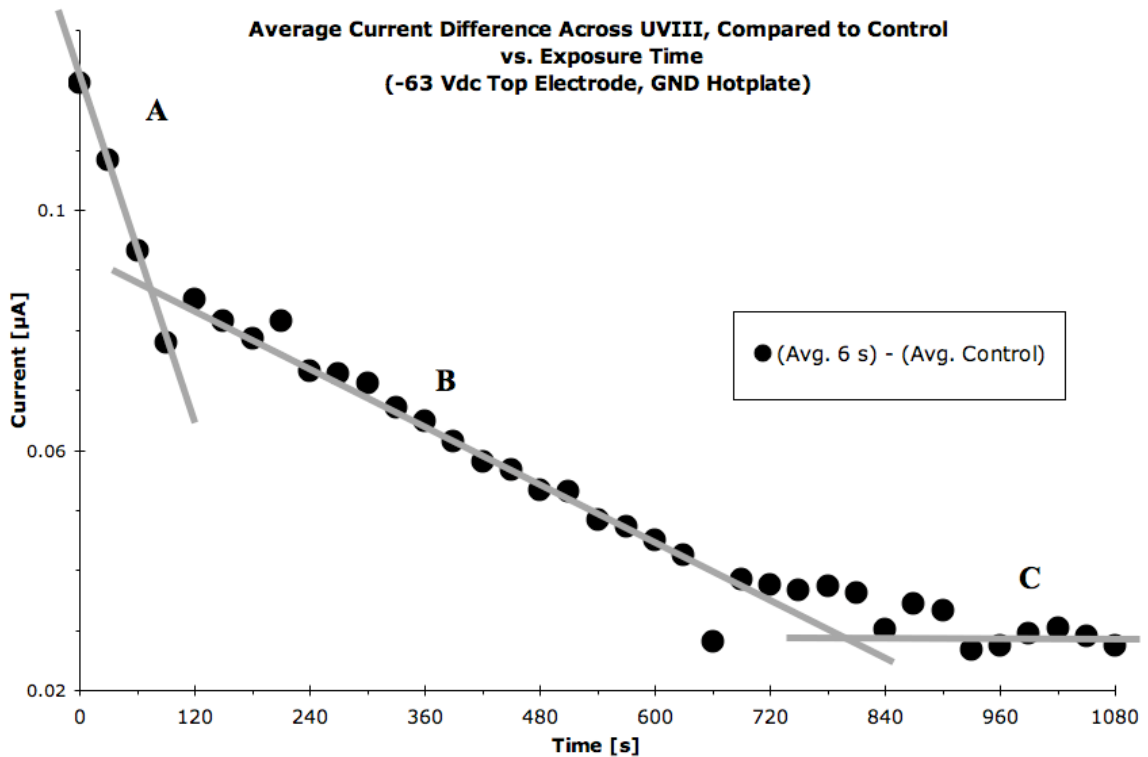
Fig. 4.5. Ion current data divided into three zones: A) electrostatic force acting on evenly distributed photogenerated acid causes charge to pile up at the interface, decreasing the current; B) acid movement diminishes due to a reduced electric field strength caused by charge separation; and C) electron current.

Around 840 s, when zone C best describes the data, the current's rate of change is zero and what is measured is due to electron drift between the electrodes. There is a difference in this final current between exposure levels visible in Fig. 4.4, which suggests

an enduring effect of exposure on acid mobility; the enhanced current associated with the larger exposure level is attributed to a greater increase in free volume as the polymer matrix is degraded by the photoacid during the deprotection reaction [16]. Zone A, which describes the first minute and a half to two minutes of the EFE-PEB, shows the fastest decline in Fig. 4.5. At zero seconds, the current is initially high because the acid is evenly distributed and begins to move all at once. The current decreases quickly as charge piles up at the interfaces and reduces the electric field strength in the photoresist via charge separation. As the plot transitions into zone B, the charge has separated and the measured current is due to acid recombination at the cathode, which decreases with the number of acid molecules.

4 different procedures were followed in an attempt to automate data collection and ultimately increase the current measurement frequency. A LabView program was written to interface with the Keithley power source, but all measurements eventually lapsed into a sinusoidal trend that swung between +2E-7 A and -2E-7 A; this occurred regardless of resist type, bake temperature, or exposure dose. Aglent software was used to interface a multimeter in series with the anode and cathode to an Excel spreadsheet; repeated measurements of unexposed UVIII followed the same trend as the previous ion current experiment, but the noise was significant. Measurements of exposed photoresist were noisy to the extent that a single trend could not be favored over other slopes. An HP4145 was intended to apply a bias and measure current over time, but curiously measured compliance—20 mA—when connected to a plugged in hotplate, 100's of nA when connected to an unplugged hotplate, and compliance when connected to an unplugged hotplate grounded to a copper pipe. Compare this data to 100's of pA with

both SMUs unconnected. Data was also taken via an MDC CV/IV measurement system; it recorded a static 1.0 μA with -50V applied to a wafer top electrode placed on unexposed resist, compliance—1 mA—over a range of 50 V to 10 V applied over both exposed and unexposed resist using a metal top electrode, and a static 1.0 μA with 5 V applied to a metal top electrode over exposed resist.

4.2   Charge Separation

As it is used in all of the experimental setups, the photoresist acts as a dielectric between the two parallel sheet electrodes and its presence will weaken the applied field within it. The effect of an electric field on nonpolar and polar dielectrics is illustrated in Fig. 4.6 and Fig. 4.7 where E_0 represents the applied electric field.

In both cases (nonpolar and polar), Gauss's law can be used to show why the field strength internal to the parallel plate capacitor is reduced by a factor equal to the relative static permittivity.

With the exception of the charges nearest the electrodes, each charge is canceled out by the opposite charge adjacent to it. The outside charges create another electric field opposing the applied field and solely existing within the dielectric. This action is illustrated in Fig. 4.8 where E' represents the secondary internal electric field.
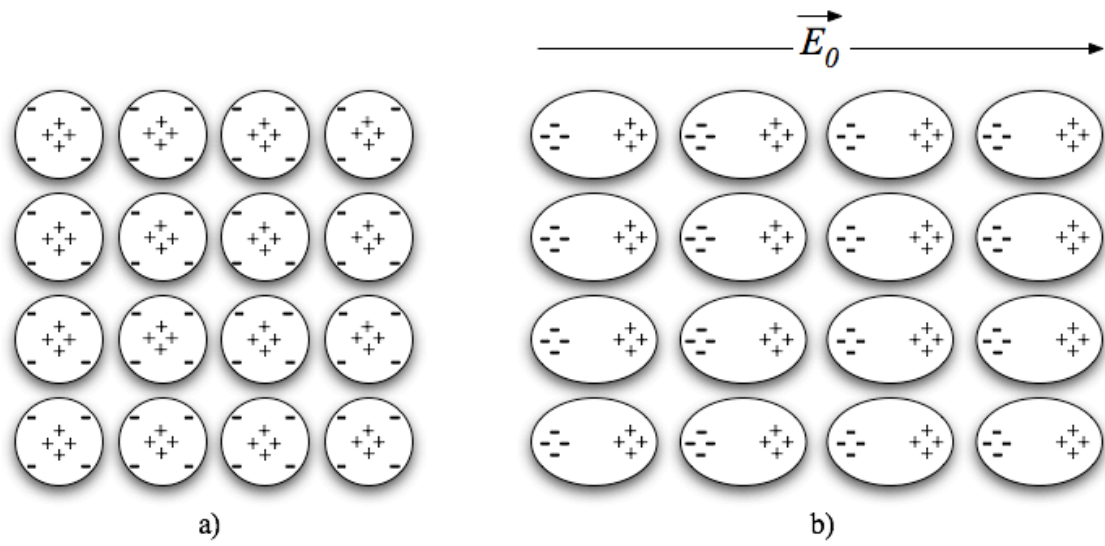
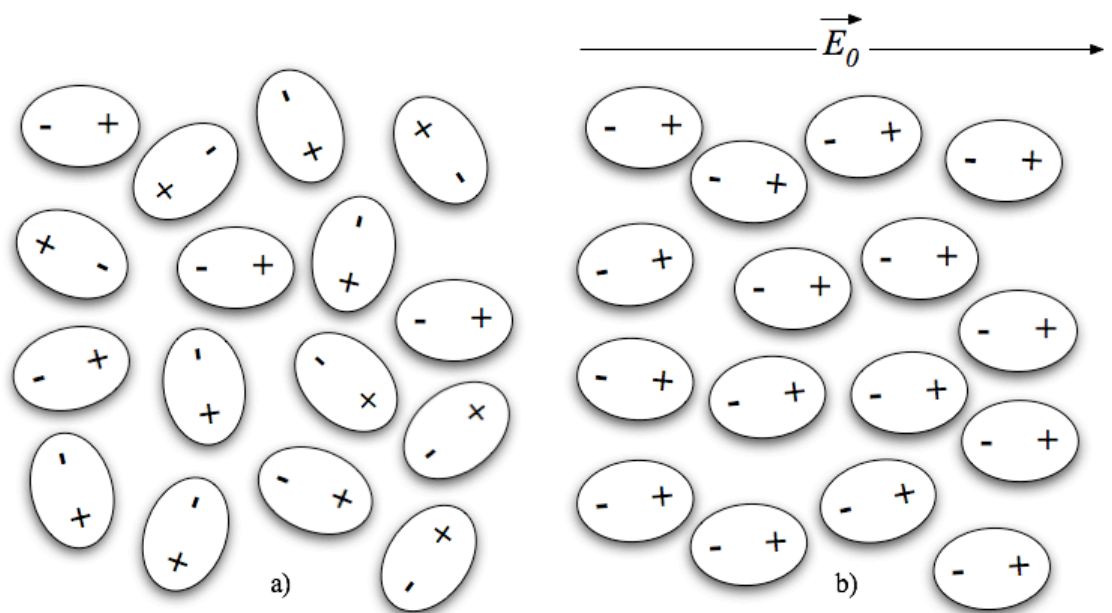Fig. 4.6. Charge location in a nonpolar dielectric a) without and b) with an applied electric field E_0.

Fig. 4.7. Charge location in a polar dielectric a) without and b) with an applied electric field E_0.
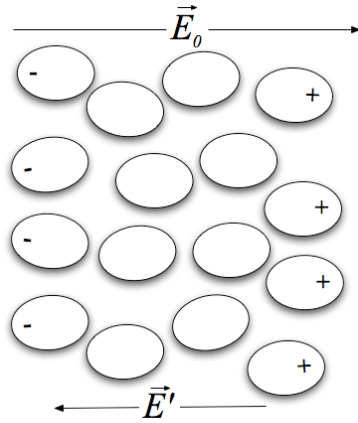
Fig. 4.8. Diagram of charges in a dielectric under the influence of an electric field E_0, creating an internal electric field E'. Canceled out charges are not drawn.

Integrating the electric field along a Gaussian surface defined around one electrode interface, as shown in Fig. 4.9, results in the electric flux. In the case of a closed Gaussian surface, the flux is equal to the enclosed charge as shown in equations 21 and 22; where q is the charge on one electrode, q' is the opposite charge induced in the dielectric, and E is the equivalent field through the photoresist; without and with the presence of a dielectric, respectively.

Fig. 4.9. Gaussian surface placed around an electrode a) without and b) with the presence of a dielectric.

$$\varepsilon_0 \oint \vec{E} \cdot d\vec{A} = \varepsilon_0 E_0 A = q, \quad E_0 = \frac{q}{\varepsilon_0 A} \tag{21}$$

47

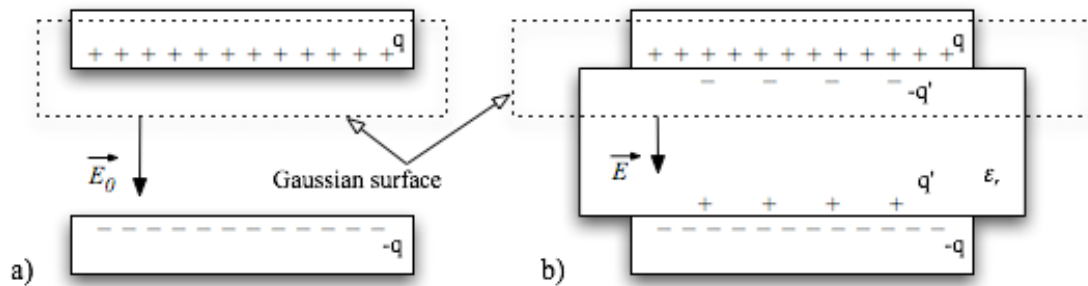$$\varepsilon_0 \oint \vec{E} \cdot d\vec{A} = \varepsilon_0 E A = q - q', \quad E = \frac{q - q'}{\varepsilon_0 A} \tag{22}$$

The only difference between equations 21 and 22 is the inclusion of q'. Equating the ratio of q to the difference between q and q' to a constant K, shown in equation 23, leads to equation 24 when applied to equation 22.

$$K \equiv \frac{q}{q - q'} \tag{23}$$

$$E = \frac{q/K}{\varepsilon_0 A} \tag{24}$$

Applying equation 21 to equation 24 leads to the relationship shown in equation 25. The relative static permittivity of a dielectric can be expressed as the ratio of the applied electric field to the equivalent internal electric field, shown in equation 26, which is equivalent to K in equation 25. This simplifies to equation 27 and leads to the form of Gauss's law shown in equation 28.

$$E = \frac{E_0}{K} \tag{25}$$

$$\varepsilon_r \equiv \frac{E_0}{E} \tag{26}$$

$$E = \frac{q}{\varepsilon_r \varepsilon_0 A} \tag{27}$$

$$\varepsilon_0 \oint \varepsilon_r \vec{E} \cdot d\vec{A} = q \tag{28}$$

The reduced strength of the field internal to the dielectric is illustrated in Fig. 4.10.
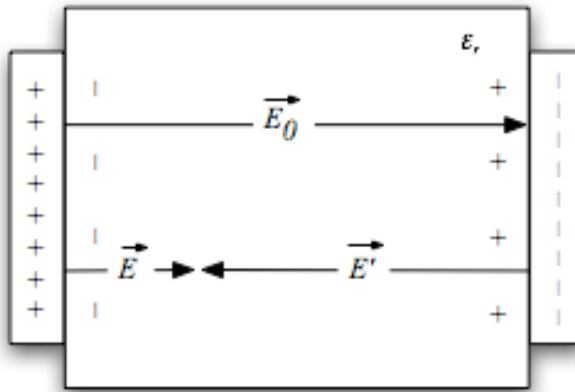
Fig. 4.10. Summation of the applied electric field and opposing internal electric field vectors. The result is a diminished vector in the direction of the applied field.

Because the presence of polar molecules makes for a more efficient dielectric, the level of exposure dose, which creates dipoles via the PAG, increases the value of the relative static permittivity, which in turn reduces the electric field strength. As is shown in Fig. 4.11, the roll of the drift length vs. diffusion length becomes increasingly lost in the thermal noise as the relative static permittivity increases. The EFE-PEB conditions are identical to Fig. 2.2 for comparison.

To relate the trend evident in Fig. 4.11 to the trend shown by the ion current experiment results, the initial electric current will be negatively driven by exposure via an increase in relative static permittivity decreasing the electric field internal to the photoresist; this is, however, overwhelmingly countered by an increase in the number of mobile charges, which drives up the current level.
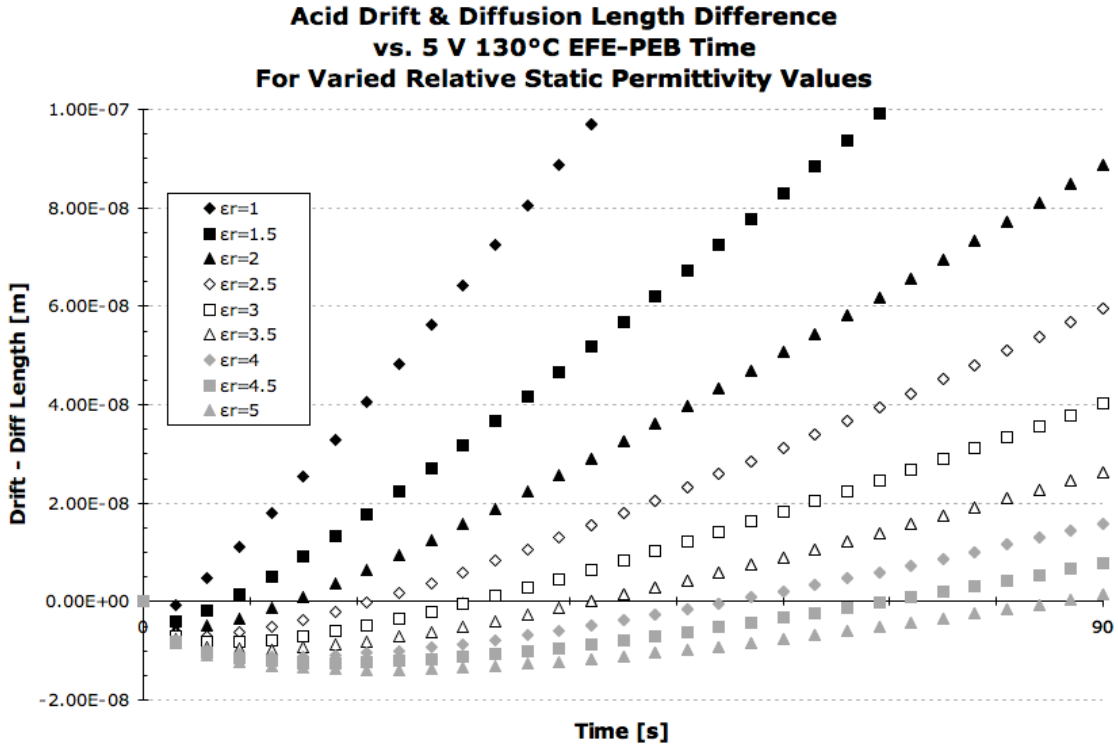
Fig. 4.11. The effect of relative static permittivity on drift length in comparison to thermal diffusion.

Despite these physical limitations on the magnitude of anisotropic movement that can be induced in the acid catalyst, researchers have published results of similarly goaled experiments including evidence of some changes in the photoresist response.

4.3   Historical Successes

As reported in the Rationale chapter, [5]–[7] and [9] give an account of dissimilar printed features measured on wafers processed with an EFE-PEB vs. a PEB. References [5]–[6] report a steeper sidewall angle and increased imaging at low exposure dose in UVIIHS exposed with electron-beam radiation, which is attributed to a reduction in horizontal acid diffusion. Reference [7] reports more complete resist removal and wider

space openings in UVIIHS underexposed with 248 nm radiation; sidewall angle results were varied. Reference [9] reports a dramatically more complete develop and reduced dose-to-clear in Apex-E photoresist exposed with 248 nm radiation, as was shown in Fig. 1.6 and Fig. 1.7. These results cannot be confirmed with the experimental techniques described in Chapter 3 because the 254 nm lamp used for all of the exposures is controlled with a simple manual on/off switch, and does not provide precise exposure control which is compounded by the bulb's spatial and temporal flux in intensity.

All of the referenced publications utilized either UVIIHS or Apex-E photoresists to demonstrate performance differences between EFE-PEB and PEB. The greatest success of the 4 publications, [9], used a topcoat to block contamination from the electrode and exploited the high acid mobility of Apex-E photoresist, which is no longer manufactured, to double focus latitude and reduce dose-to-clear by 8%. Reference [17] measured acid mobility in Apex-E at 1×10^{-3} μm^2/s. UVIIHS, out of [5]–[7], exhibited the most pronounced acid diffusion enhancement in [7], which in turn referenced its acid mobility at 9×10^{-6} μm^2/s. The acid mobility of UVIIHS, a environmentally stable chemically amplified photoresist (ESCAP), is 3 orders of magnitude smaller than Apex-E. This is because ESCAP resists contain a PAG with strongly associating anion and cation components and are densified at the softbake to decrease free volume, which reduces susceptibility to airborne base contamination [18]. As a consequence of these limiting factors, the experimental results using UVIIHS were less prominent compared to results garnered from Apex-E. As was reported in [7], resist spaces became wider and deeper with EFE-PEB vs. PEB—results similar to increasing the exposure dose.

In the case of each photoresist, differences between PEB and EFE-PEB were most

evident for small space widths. In [9], differences between control and experimental were reported as insignificant for 420 nm and 500 nm spaces, while 337 nm features exhibited the results discussed earlier. In [7], both 300 nm and 400 nm spaces increased by 46 nm as measured at the resist surface, while 300 nm spaces narrowed by 29 nm and 400 nm spaces widened by 9 nm at the base. Changes in post develop dimension remained constant with respect to mask feature size at the resist surface because acid displacement is only a factor of electric field strength, temperature, and mobility. These results can be compared to Table II, which reports the maximum thickness loss difference between control and experimental conditions, achieved in the third experimental setup, as 26.9 nm.

The last 2 experimental setups differed from [5]–[7] and [9] in that, as illustrated in Fig. 4.12, acid ions were generated throughout the resist, as opposed to being patterned. In addition, to create alternating areas of EFE-PEB and PEB, the top electrode used in the last 2 experimental setups was designed to only apply discrete, isolated sections of bias relative to the uniform bottom electrode. Compared to the mirror-image electrode configuration of [5]–[7] and [9], this uneven setup does not deliver parallel field lines and will apply a small horizontal drift velocity to catalyst ions in the PEB portion of the experiment; this is further evidence counter to the third assumption stated in section 4.1.
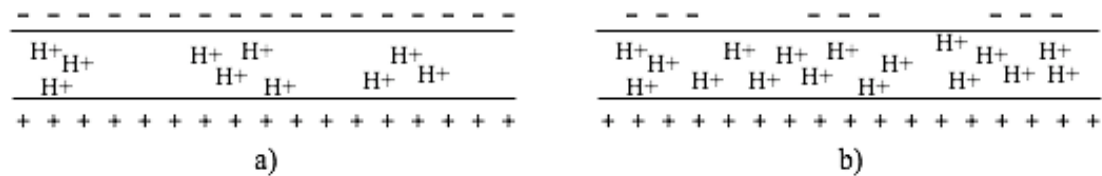

Fig. 4.12. Location of charges in a) [5]–[7] and [9], and b) the second and third experimental setup.

Chapter 5

Conclusions

5.1 Summary of Notable Consequences and Causes

Over three major experimental design iterations, the magnitude of thickness loss enhancement caused by the addition of an electric field to exposed chemically amplified resist during a post exposure bake increased with each successful evolution as measured by profilometry increasing from less than 10 nm to more than 20 nm of additional thickness loss over control. At an early stage of the series of experiments, 86 nm thickness loss enhancement was measured via AFM; this result did not reproduce with repetition. Repeatability was a problem throughout, which is attributed to variations in the electrode gap, which could be caused by a large photoresist thickness standard deviation, particle contamination, or outgassing as solvent evaporates during the bake, and introduction of base contamination from the top electrode which was in contact with the photoresist. During AFM, a section of resist was found to have overlapped over on its self; this calls into question whether the profilometry measurements represent thickness loss variation or folded photoresist coincidentally matching the pitch of the top electrode.

Two out of the three base assumptions were shown to be false: it was proven that acid concentration is not constant over time during the EFE-PEB, and electric field strength is not zero beneath control regions of the 10 μm pitch top electrode. The latter was proved through current measurements across the top electrode insulator. The former was determined by measuring current between the anode and cathode; the current trend over time suggests a swift charge separation caused by acid pileup at the

electrode/photoresist interfaces followed by a slower process of acid neutralization by electrons from the cathode until the current equalizes at the level of electron drift across the dielectric.

5.2   Recommendations, Musings, and Retrospection

This work differs from [9], the most successful previous attempt, in several key design characteristics: the resist was flood exposed and enhanced in periodic strips with an intermittent electric field opposed to being patterned with radiation and enhanced uniformly; ESCAP was used instead of a high acid mobility resist like Apex-E; topcoat, which would prevent contamination on the top electrode from poisoning the acid catalytic reaction when it comes into contact with the photoresist, was not available, and the hardbaked acid barrier on the top electrode spent considerable time exposed to laboratory air during other processing. Base contamination from the top electrode is known to exist because each processing day was made to start with repeated EFE-PEB experiments that showed a gradual reduction in thickness loss suppression, reran until the action ceased, in order to minimize the effect.

There are variations on the same experimental setup that could tweak the results without requiring reexamination of theory or construction of a new apparatus. A transparent and conductive topcoat would serve as a top electrode free of contamination and match electrode gap variation to the dielectric thickness standard deviation. As another example, if CAR were coated over resist lacking a PAG and an electric field applied so as to drive photogenerated acid into the bottom layer, any thickness loss

greater than a control PEB can be attributed to the field; this could be accomplished with a flood exposure if the radiation intensity were spatially uniform.

There are other ways in which anisotropic acid catalyst displacement can manifest itself. LWR measurements, critical dimension and dose-to-clear swing curves, and contrast curves all can be used to derive process parameters that depend on acid diffusion and standing waves that would obviate any orderly changes in acid catalyst movement.

Notable attention was paid to reducing acid neutralization by electrons at the cathode. Even though this action reduces the number of ions available to deprotect the photoresist, perhaps acid neutralization would prevent charge pileup at interfaces and thus increase the total acid displacement. It is also possible that a large enough voltage placed across the photoresist would cause the acid to drift too quickly to deprotect the polymer; that is, not enough time elapses for the acid to interact with the appropriate chemical bond. This scenario should be evaluated with chemical kinetics and thermodynamics.

Chapter 6

References

[1]   International Technology Roadmap for Semiconductors: http://public.itrs.net

[2]   J. Zhou, Y. Fan, B. W. Smith, "Three-dimensional imaging of 30-nm nanospheres using immersion interferometric lithography," *Proc. of SPIE: Optical Microlithography XIX*, vol. 6154, 2006.

[3]   *UVIII™ Positive DUV Photo Resists*, Shipley Company, Marlborough, MA, 1997.

[4]   B. W. Smith, Y. Fan, J. Zhou, N. Lafferty, A. Estroff, "Evanescent wave imaging in optical lithography," *Proc. of SPIE: Optical Microlithography XIX*, vol. 6154, 2006.

[5]   M. Cheng, E. Croffie, L. Yuan, and A. Neureuther, "Enhancement of resist resolution and sensitivity via applied electric field," *J. Vac. Sci. Technol.,* B 18(6), 2000.

[6]   M. Cheng, L. Yuan, E. Croffie, and A. Neureuther, "Improving resist resolution and sensitivity via electric-field enhanced postexposure baking," *J. Vac. Sci. Technol.,* B 20(2), 2002.

[7]   M. Cheng, J. Poppe, and A. Neureuther, "Effects of treatment parameters in electric-field-enhanced postexposure bake," *J. Vac, Sci, Technol.,* B 21(4), 2003.

[8]   M. Cheng, and A. R. Neureuther, "Method and apparatus for enhancing resist sensitivity and resolution by application of an alternating electric field during post-exposure bake," U.S. Patent 6 686 132, February 3, 2004.

[9]   J. Poppe, and A. R. Neureuther, "Improved performance of Apex-E photoresist with the application of the electric field enhanced PEB," *Proc. of SPIE: Advances in Resist Technology and Processing XXI*, vol. 5376, 2004.

[10]   V. Constantoudis, G. P. Patsis, L. H. A. Leunissen, and E. Gogolides, "Line edge roughness and critical dimension variation: fractal characterization and comparison using model functions," *J. Vac. Sci, Technol.,* B 22(4), 2004.

[11]   J. Foucher, A. L. Fabre, and P. Gautier, "CD-AFM vs CD-SEM for resist LER and LWR measurements," *Proc. of SPIE: Metrology, Inspection, and Process Control for Microlithography XX*, vol. 6152, 2006.

[12]   H. Ito, "Dissolution behavior of chemically amplified resist polymers for 248-, 193-, and 157-nm lithography," *IBM J. Res. & Dev.*, vol. 45, no. 5, September 2001.

[13]   D. Kang, E. K. Pavelchek, and C. Swible-Keane, "The accuracy of current model descriptions of a DUV photoresist," *SPIE Conference on Advances in Resist Technology and Processing XVI*, vol. 3678, 1999.

[14]   *UV6™ Positive DUV Photoresist for DUV Applications*, Rohm and Haas Company, Philadelphia, PA, 2004.

[15]   T. A. Brunner, N. Seong, W. D. Hinsberg, J. A. Hoffnagle, F. A. Houle, and M. I. Sanchez, "High numerical aperture lithographic imagery and the Brewster angle," *SPIE J. Microlithography, Microfabrication, and Microsystems*, vol. 1, issue 3, pp. 188-196, 2002.

[16]   J. L. P. Jessop, S. N. Goldie, A. B. Scranton, G. J. Blanchard, B. Rangarajan, L. Capodieci, R. Subramanian, and M. K. Templeton, "Characterizing acid mobility in chemically amplified resists via spectroscopic methods," *SPIE Conference on Advances in Resist Technology and Processing XVI*, vol. 3678, 1999.

[17]   L. Yuan and A. Neureuther, "Improving chemically-amplified resist modeling for 2D layout patterns," *Proc. of SPIE: Advances in Resist Technology and Processing XX*, vol. 5039, 2003.

[18]   K. R. Dean, D. A. Miller, R. A. Carpio, J. S. Petersen, and G. K. Rich, "Effects of airborne molecular contamination on DUV photoresists," *J. Photopolymer Sci. Technol.*, vol. 10, no. 3, 1997.